Postharvest Biology and Technology 243 (2027) 114675

Contents lists available at ScienceDirect

Postharvest Biology and Technology

journal homepage: www.elsevier.com/locate/postharvbio

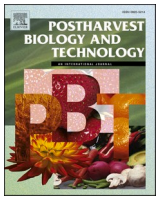

An integrated dynamic model of ethylene biosynthesis and respiration of 'Conference' pear (*Pyrus communis*) during storage and shelf life

Hoang Minh Phan [a], Bert E. Verlinden [b], Pieter Verboven [a], Maarten L.A.T.M. Hertog [a,*], Bart M. Nicolaï [a,b]

[a] KU Leuven, BIOSYST-MeBioS, Leuven, Belgium
[b] Flanders Centre of Postharvest Technology, Leuven, Belgium

ARTICLE INFO

Dataset link: Replication Data for: An integrated dynamic model of ethylene biosynthesis and respiration of 'Conference' pear (Pyrus communis) during storage and shelf life

Keywords:
Dynamic Controlled Atmosphere
Pear Storage
Fruit Ripening
Kinetic Modelling
Michaelis-Menten Kinetics

ABSTRACT

Respiration and ethylene biosynthesis rates change dynamically in maturing and ripening climacteric fruit. However, typically in modelling work, under low-temperature controlled atmosphere storage, the temporal changes of these metabolic processes have often been neglected. This paper proposes a simplified modelling approach to describe and integrate the temporal changes of respiration and ethylene biosynthesis during storage and subsequent shelf-life. The model starts from transcriptome levels of the involved enzymes and incorporates enzyme synthesis and degradation. The interaction between oxygen and ethylene metabolism at the pathway and signalling level is explicitly incorporated in the kinetic equations. These dynamic models of respiration and ethylene biosynthesis were calibrated using mainly shelf-life data (18 °C in regular air) obtained after storage under various conditions. The models were then validated using data from a storage experiment under standard CA (-1 °C, 3 kPa O_2, 0.7 kPa CO_2) and DCA (-1 °C) conditions in both laboratory and industry settings. The goodness of fit, expressed by the adjusted coefficient of determination R^2_{adj}, for the coupled model of ethylene and respiration was 0.68. Overall, the model was able to capture the dynamic pattern of respiration and ethylene biosynthesis, aligning acceptably with the measured data in shelf-life. Specifically, the exchange rate of respiratory gases generally increases and stabilises after one week in shelf-life, while the peak of the ethylene exchange rate usually shifts earlier with later shelf-life stages from different storage conditions.

1. Introduction

Controlled atmosphere (CA) storage is effective for retaining pear fruit quality after harvest (Saltveit, 2003; Prange, 2018). In traditional CA, O_2 and CO_2 partial pressures are maintained at steady levels, which for Belgian 'Conference' pear are 3 kPa O_2 and 0.7 kPa CO_2 at −1 °C (Schenk, 2024). Dynamic controlled atmosphere storage (DCA) involves dynamically controlling the O_2 level over the storage period by measuring fruit physiological responses based on either respiration quotient (RQ, the ratio of CO_2 production rate to O_2 consumption rate), chlorophyll fluorescence, or ethanol production (Mditshwa et al., 2018). The resulting O_2 level in DCA is generally lower than in CA. As a result of the low O_2 conditions created by CA and DCA, fruit respiration and ethylene biosynthesis are repressed, slowing down quality deterioration processes (Alexander and Grierson, 2002; Pattyn et al., 2021).

Although (dynamic) controlled atmosphere, referred to as (D)CA, can retain quality during long-term storage, challenges still remain. As pear is a climacteric fruit, ripening still progresses during long-term storage, so that fruit at different commercialisation times enters the market in different physiological states. Commonly, fruit quality is evaluated through physicochemical attributes such as firmness, background colour, soluble solids content and titratable acidity, as well as the incidence of storage disorders, for example, internal browning (Kappel et al., 1995; Eccher Zerbini, 2002; Franck et al., 2007). These attributes are the outcomes of underlying metabolic processes, among which ethylene biosynthesis plays a central role (Barry and Giovannoni, 2007; Villalobos-Acuña and Mitcham, 2008; Liu et al., 2015). Additionally, cold storage also consumes energy from refrigeration, directly proportional to the respiration heat (Phan et al., 2026b). Therefore, understanding the related changes in respiration and ethylene biosynthesis during (D)CA storage is vital to better control pear fruit quality and energy consumption during and/or after (D)CA storage.

However, to this end, quantitative tools that can monitor and predict fruit quality and energy consumption are needed to support storage

* Corresponding author.
E-mail address: maarten.hertog@kuleuven.be (M.L.A.T.M. Hertog).

https://doi.org/10.1016/j.postharvbio.2026.114675
Received 18 March 2026; Received in revised form 27 July 2026; Accepted 20 August 2026

decisions under different operating scenarios. This is complicated by the fact that both ethylene biosynthesis and respiration are dynamic and depend nonlinearly on storage conditions and duration. Consequently, the outcome of new storage conditions would be difficult to infer by interpolating between individual experiments, while experimenting with the full range of operating conditions would be expensive. Kinetic models resolve this by expressing these dependencies as rate equations, which allow for scenario analysis, extrapolation beyond the conditions actually sampled, and process optimisation, while reducing the labour cost of routine quality monitoring and circumventing the safety risk associated with entering low-oxygen (D)CA rooms.

For respiration, Michaelis-Menten-based models are the gold standard and have been applied to a variety of fruit, for example, tomato (Sousa et al., 2017; Xiao et al., 2024), apple (Lakakul et al., 1999; Ho et al., 2013), pear (Lammertyn et al., 2003; Ho et al., 2008), strawberry (Jalali et al., 2020), dragon fruit (Ho et al., 2020), and litchi fruit (Mangaraj and Goswami, 2011). The Michaelis-Menten approach simplifies the complex respiration metabolism into a process regulated by a single rate-limiting enzyme. By introducing different inhibition mechanisms of CO_2 on the substrate and/or the substrate-enzyme complex, such as competitive, uncompetitive, and non-competitive inhibition, the Michaelis-Menten model has become suitable for modelling the respiration kinetics of fruit and vegetables based on data obtained from typical lab-controlled experiments in air-tight jars (Peppelenbos and Van'T Leven, 1996). With the Michaelis-Menten model, fruit respiration can be predicted as a function of the gas composition (O_2 and CO_2) in storage. To describe the effect of temperature, the Arrhenius law is usually integrated (Hertog et al., 1998; Fonseca et al., 2002). Besides Michaelis-Menten, a first-order chemical kinetics approach can also be used for respiration modelling to reduce the non-linearity in the Michaelis-Menten equation (Wang et al., 2009). Furthermore, a black-box modelling approach, though not recommended because of a lack of any mechanistic foundation, may be applied to model fruit respiration using a simple polynomial expression (Barbosa et al., 2018). Despite the fact that the Michaelis-Menten approach is commonly used, its main drawback is the absence of any time effects, such as ripening-related changes. Since respiration changes over time due to climacteric fruit ripening, a dynamic respiration model is indispensable to characterise the full respiration behaviour of ripening fruit. One of the few respiration models, including time effects, considered the transcriptional regulation of the maximum respiration rate in response to hypoxia (Ho et al., 2018). Recently, another modelling effort has been made for respiration dynamics using storage conditions with a simple enzymatic framework (Phan et al., 2026a). However, none of them included the effect of ethylene on the respiration evolution.

Ethylene biosynthesis is more complex to model because of its autocatalytic mechanism driven by downstream signalling and multi-level control (Alexander and Grierson, 2002; Binder and Jez, 2020; Pattyn et al., 2021). Ethylene biosynthesis has been modelled using a simplified Michaelis-Menten approach (De Wild et al., 1999), but with the abovementioned drawback of lacking time dependencies. Génard and Gouble (2005) developed a dynamic model for ethylene biosynthesis in peaches, which showed an acceptably accurate prediction of ethylene emission to the environment. This model considered ethylene biosynthesis at a metabolomic level and incorporated the change of different metabolites in ethylene biosynthesis, such as S-adenosyl-L-methionine (SAM), 1-Aminocyclopropane-1-carboxylic acid (ACC), and malonyl-ACC (MACC). Van de Poel et al. (2014) extended this approach to the transcriptome level while modelling ethylene biosynthesis in tomatoes. Herein, the authors modelled how ACC synthase (ACS) and ACC oxidase (ACO), i.e., enzymes involved in ethylene biosynthesis, are biosynthesised using gene expression levels as model inputs. Nguyen et al. (2025) validated this model at the protein level and further extended it by including ethylene signalling. Although these models provide insights into multiple levels of ethylene biosynthesis, they are too complex to be implemented in practice because of the large amount of data required to calibrate the models. There were attempts to simplify the complexity of modelling ethylene biosynthesis by Gwanpua et al. (2014, 2017). Briefly, their approach was to introduce the climacteric state to model the autocatalytic mechanism in ethylene biosynthesis and senescence process while simply keeping the enzymatic reactions based on the Michaelis-Menten approach. The prediction seemed acceptable, but the approach was overly simplified and failed to capture the enzymatically mechanistic complexity of ethylene biosynthesis. As a result, the model applicability is likely limited to the different use cases on which the model was calibrated.

This paper aims to introduce a simple and general concept for modelling the dynamics of respiration and ethylene biosynthesis in climacteric fruit, not only as a function of changing storage conditions but also addressing its time dependency, accounting for the dynamics of the underlying regulatory processes. The developed models are calibrated and validated at various temperatures and gas conditions to demonstrate the model robustness, covering both storage and shelf life of 'Conference' pear. Finally, the model is used to illustrate the effect of RQ-DCA and CA conditions on respiration and ethylene biosynthesis.

2. Material and methods

2.1. Model development

2.1.1. Modelling framework

Fig. 1 shows a reaction scheme linking ethylene biosynthesis and respiration together, and presents its process at the tissue level of the pear. In general, the coupled model integrates both processes within the fruit tissue, where the metabolic gases permeate through the pear skin according to its permeability. The ethylene biosynthesis submodel describes the dynamics of two enzymes, ACS and ACO, explicitly. Furthermore, modelling the dynamics of ACS is extended to the transcriptomic level. The ethylene biosynthesis submodel requires the internal O_2 as an input for ethylene biosynthesis. The internally produced ethylene then acts as a signal to stimulate the respiration of the fruit. Since O_2 is also a substrate for the respiration process, the internal O_2 level is also regulated by the respiration submodel. As a result, a feedback loop between the two submodels is created through internal O_2 and ethylene. Consequently, the exchange rates of ethylene and respiratory gases are indirectly linked through metabolic substrates (such as ethylene and O_2) and their corresponding enzymes. To limit the scope and complexity of the model, we assumed that the gas concentrations inside the fruit were homogeneous. In addition, individual enzyme isoforms were not explicitly considered. Instead, the model addresses the net effects of gene expression and enzyme activity, adapted from Nguyen et al., (2025). This simplification was introduced not to involve isoform-specific regulation with regard to gene expression levels and enzyme activities. The model, therefore, focuses on an aggregate regulation, rather than an isoform-specific regulation. This approach should enhance its generic value. More details on the two submodels and their corresponding assumptions are described in Section 2.1.2 for ethylene biosynthesis and Section 2.1.3 for respiration. All symbols in our model development are present in Table 1.

2.1.2. Dynamics of ethylene biosynthesis

Ethylene biosynthesis can be regulated through two different systems: system 1 governing the growth and development phase of fruit, and system 2 ruling floral senescence and fruit ripening (Alexander and Grierson, 2002). The latter is crucial in a postharvest context since it is an autocatalytic process. Ethylene biosynthesis starts from S-adenosyl-L-methionine (SAM), a metabolite in the Yang cycle. Under the catalysis of ACC synthase (ACS), SAM is converted to 1-aminocyclopropane-1-carboxylic acid (ACC). Then, ethylene is produced from ACC, catalysed by ACC oxidase (ACO) in the presence of O_2. When ethylene is present in the fruit, it binds to ethylene receptors. This triggers the ethylene-signalling pathway, which is a complex process related to

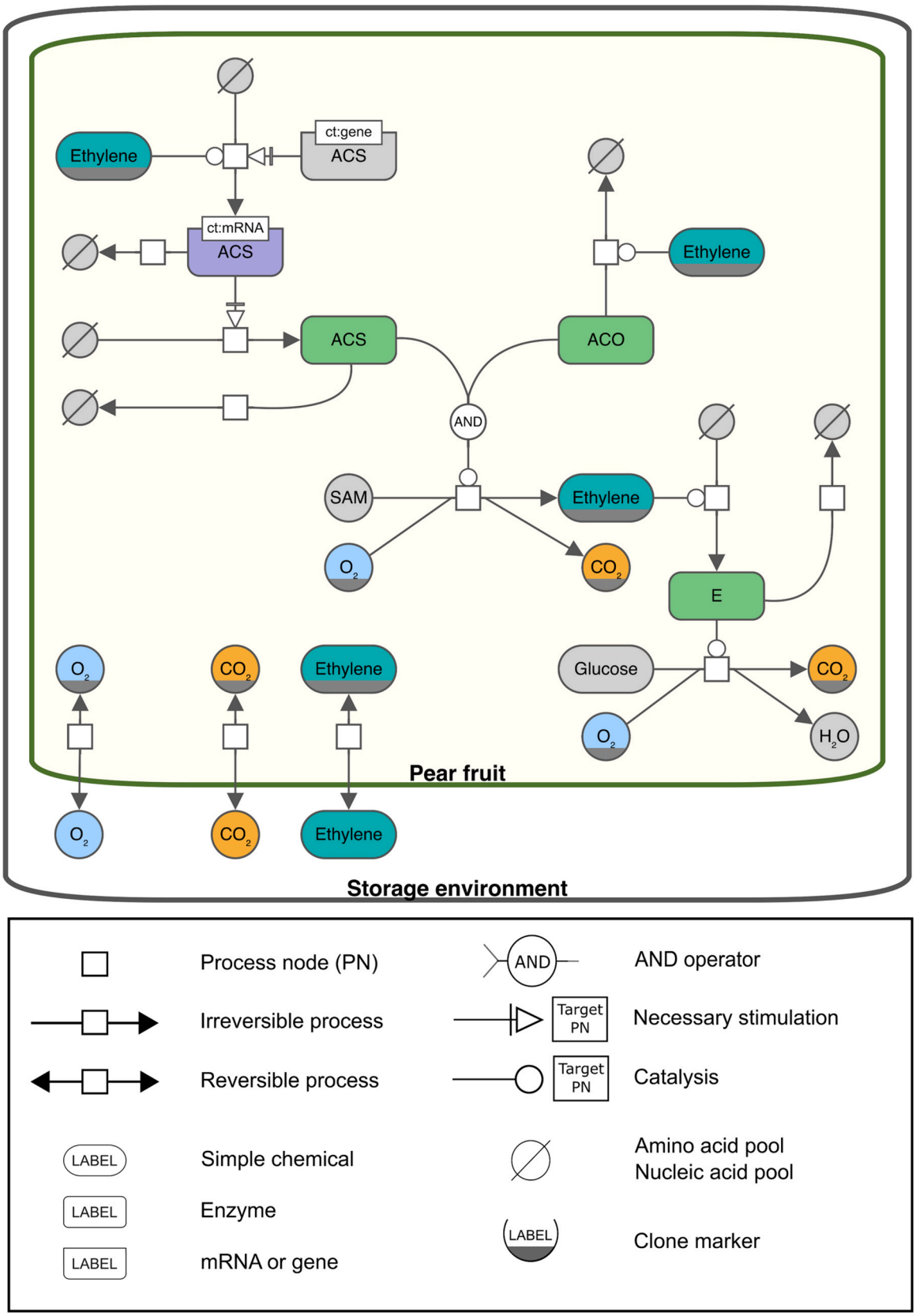

Fig. 1. Theoretical framework for modelling the dynamics of ethylene biosynthesis and respiration rate of 'Conference' pear, in which SAM represents S-adenosyl-L-methionine, ACS represents ACC synthase, ACO represents ACC oxidase in ethylene biosynthesis, and E_r represents the respiration process lumped as a single enzyme. This scheme follows the SBGN standard (Sari et al., 2015; Balci et al., 2021).

Table 1
List of symbols in model description.

Symbol	Unit	Description
Pear parameters		
A_p	m^2	Surface area of pear skin
V_p	m^3	Pear volume
m_p	kg	Pear mass
ρ_p	kg m^{-3}	Pear density
P_{Eth}	m s^{-1}	Permeability coefficient of ethylene through pear skin
P_{O2}	m s^{-1}	Permeability coefficient of O_2 through pear skin
P_{CO2}	m s^{-1}	Permeability coefficient of CO_2 through pear skin
Model state variables		
[Eth]	mol m^{-3}	Ethylene concentration inside pear
$[O_2]$	mol m^{-3}	Oxygen concentration inside pear
$[CO_2]$	mol m^{-3}	Carbon dioxide concentration inside pear
$[Eth]_\infty$	mol m^{-3}	Ethylene concentration outside pear
$[O_2]_\infty$	mol m^{-3}	O_2 concentration outside pear
$[CO_2]_\infty$	mol m^{-3}	CO_2 concentration outside pear
$[mRNA_{ACS}]$	mol m^{-3}	Concentration of mRNA for ACS transcription
[ACS]	mol m^{-3}	ACS concentration
[ACO]	mol m^{-3}	ACO concentration
[E]	mol m^{-3}	Concentration of a lumped enzyme for respiration
Model parameters of the ethylene biosynthesis		
$R_{Eth,max}$	mol $m^{-3}s^{-1}$	Maximum ethylene production rate
k_{Eth}	m^3 $mol^{-1}s^{-1}$	Rate constant of ethylene biosynthesis
$k_{RNA,syn}$	mol $m^{-3}s^{-1}$	Rate constant of transcription process of $mRNA_{ACS}$
$k_{RNA,deg}$	s^{-1}	Rate constant of degradation of $mRNA_{ACS}$
$k_{ACS,syn}$	s^{-1}	Rate constant of ACS production
$k_{ACS,deg}$	s^{-1}	Rate constant of ACS degradation
$k_{ACO,deg}$	m^3 $mol^{-1}s^{-1}$	Rate constant of ACO degradation
$k_{d,Eth}$	s^{-1}	Overall diffusion constant of ethylene through fruit skin
$K_{m,Eth}$	mol m^{-3}	Michaelis-Menten constant for ethylene biosynthesis
K_{RNA}	mol m^{-3}	Michaelis-Menten constant for $mRNA_{ACS}$ production
$E_{a,Eth}$	J mol^{-1}	Activation energy of k_{Eth}
$E_{a,RNA,syn}$	J mol^{-1}	Activation energy of $k_{RNA,syn}$
$E_{a,RNA,deg}$	J mol^{-1}	Activation energy of $k_{RNA,deg}$
$E_{a,ACS,syn}$	J mol^{-1}	Activation energy of $k_{ACS,syn}$
$E_{a,ACS,deg}$	J mol^{-1}	Activation energy of $k_{ACS,deg}$
$E_{a,ACO,deg}$	J mol^{-1}	Activation energy of k_{ACO}
Model parameters of the respiration		
$R_{O2,max}$	mol $m^{-3}s^{-1}$	Maximum O_2 consumption rate
$R_{CO2,max,f}$	mol $m^{-3}s^{-1}$	Maximum CO_2 production rate from fermentation
k_{rsp}	s^{-1}	Rate constant of the oxidative respiration process
$k_{E,syn}$	s^{-1}	Rate constant of production of respiration enzyme
$k_{E,deg}$	s^{-1}	Rate constant of degradation of respiration enzyme
$k_{d,O2}$	s^{-1}	Overall diffusion constant of O_2 through fruit skin
$k_{d,CO2}$	s^{-1}	Overall diffusion constant of CO_2 through fruit skin
$K_{m,O2}$	mol m^{-3}	Michaelis-Menten constant for oxidative respiration rate
$K_{m,CO2,f}$	mol m^{-3}	Michaelis-Menten constant of fermentation
$E_{a,O2}$	J mol^{-1}	Activation energy of k_{rsp}
$E_{a,CO2}$	J mol^{-1}	Activation energy of $R_{CO2,max,f}$
$E_{a,E,syn}$	J mol^{-1}	Activation energy of $k_{E,syn}$
$E_{a,E,deg}$	J mol^{-1}	Activation energy of $k_{E,deg}$
$r_{q,ox}$		Respiratory quotient
Gas exchange rates (Model outputs)		
φ_{Eth}	mol $m^{-3}s^{-1}$	Exchange rate of ethylene
φ_{O2}	mol $m^{-3}s^{-1}$	Exchange rate of O_2
φ_{CO2}	mol $m^{-3}s^{-1}$	Exchange rate of CO_2
Other parameters and variables		
R	J $mol^{-1}K^{-1}$	Ideal gas constant
T	°C or K	Temperature
Extra subscripts		
ref		Parameters at a reference temperature
t = 0	s or d	State variables at initial time (t = 0)
Extra superscript		
*		Normalized variable or parameter[a]

[a] The unit of normalised variables or parameters is changed with respect to the used normalisation method. More details are described in the supplementary data.

transcriptions and translations of, amongst others, ACS and ACO. As a result, ethylene production increases autocatalytically (Alexander and Grierson, 2002; Barry and Giovannoni, 2007; Chang, 2016).

The Michaelis-Menten equation is often used to model ethylene biosynthesis, assuming a single enzyme that presumably lumps ACS and ACO for simplicity (De Wild et al., 1999). However, this paper explicitly includes ACS and ACO to capture the influence of the enzyme turnover on ethylene biosynthesis. This separation assumes that the changes in ACS and ACO levels result in a rapid adaptation of the enzyme-substrate complex in ethylene biosynthesis, which establishes a quasi-steady state again. Furthermore, by accounting for the ethylene diffusion through the fruit skin, the ethylene inside the fruit can be modelled as in Eq. 1 and Eq. 2.

$$\frac{d}{dt}[\mathrm{Eth}] = \frac{R_{\mathrm{Eth,\ max}}[\mathrm{O_2}]}{K_{\mathrm{m,Eth}} + [\mathrm{O_2}]} + k_{\mathrm{d,Eth}}([\mathrm{Eth}]_\infty - [\mathrm{Eth}]) \tag{1}$$

$$R_{\mathrm{Eth,\ max}} = k_{\mathrm{Eth}}[\mathrm{ACS}][\mathrm{ACO}] \tag{2}$$

where $R_{Eth,max}$ is the maximum ethylene production rate (mol $m^{-3}s^{-1}$); $K_{m,Eth}$ is the Michaelis-Menten constant (mol m^{-3}); [Eth] and $[Eth]_\infty$ are ethylene concentrations (mol m^{-3}) inside and outside the fruit, respectively, while $[O_2]$ is the oxygen concentration (mol m^{-3}) inside the fruit; k_{Eth} is a rate constant (m^3 $mol^{-1}s^{-1}$) of ethylene biosynthesis with explicit expression of ACS and ACO. [ACS] and [ACO] represent the concentrations (mol m^{-3}) of ACS and ACO, respectively; $k_{d,Eth}$ is an overall diffusion constant (s^{-1}) describing the diffusion rate of ethylene from inside the fruit toward the environment, calculated as

$$k_{\mathrm{d,Eth}} = P_{\mathrm{Eth}}\frac{A_p}{V_p} \tag{3}$$

with P_{Eth}, A_p, and V_p being pear's skin permeability (m s^{-1}) for ethylene, surface area (m^2), and fruit volume (m^3), respectively. The permeability of ethylene through pear skin (P_{Eth}) is approximated using Graham's law based on the skin permeability of oxygen P_{O2}. In case the ethylene production rate follows Michaelis-Menten kinetics without the dynamics of enzyme turnover, model (Eq. 1) is referred to as the static model of ethylene biosynthesis, as ethylene biosynthesis then only depends on O_2 availability and temperature.

The dynamic behaviour of ethylene biosynthesis is modelled through the change in ACS and ACO, each of which has its own role at different climacteric stages. It is well-known that ACS is a rate-limiting step for the autocatalytic stage of ethylene biosynthesis (Argueso et al., 2007). Furthermore, the finding of Bulens et al. (2014) on 'Jonagold' apples showed that a low transcript abundance and a rapid protein turnover strongly influence the ACS activity. Hence, increased ACS transcription (e.g., ACS1) leads to higher ACS activity and ethylene production. In contrast, their study also showed that ACO was not the rate-limiting step of ethylene production during storage. Van de Poel et al. (2012) demonstrated that ACO becomes the rate-limiting step in the post-climacteric stage of tomato, thus decreasing ethylene biosynthesis.

The dynamic behaviour of ACS is proposed in Fig. 1. Once ethylene is produced and binds to the ethylene receptor, a signalling pathway is triggered, inducing mRNA transcription for ACS synthesis. Subsequently, the $mRNA_{ACS}$ is translated to produce ACS. Additionally, the $mRNA_{ACS}$ and ACS can be degraded to nucleotides and amino acids, respectively. Based on this reaction scheme, a set of differential equations is derived as follows:

$$\frac{d}{dt}[\mathrm{mRNA_{ACS}}] = k_{\mathrm{RNA,syn}}\frac{[\mathrm{Eth}]}{K_{\mathrm{RNA}} + [\mathrm{Eth}]} - k_{\mathrm{RNA,deg}}[\mathrm{mRNA_{ACS}}] \tag{4}$$

$$\frac{d}{dt}[\mathrm{ACS}] = k_{\mathrm{ACS,syn}}[\mathrm{mRNA_{ACS}}] - k_{\mathrm{ACS,deg}}[\mathrm{ACS}] \tag{5}$$

where $[mRNA_{ACS}]$ is the mRNA concentration (mol m^{-3}) for ACS; $k_{RNA,}$

$_{syn}$ and $k_{RNA,deg}$ are rate constants for the transcription process (mol $m^{-3}s^{-1}$) and RNA degradation (s^{-1}), respectively; $k_{ACS,syn}$ and $k_{ACS,deg}$ are rate constants for ACS production (s^{-1}) and degradation (s^{-1}), respectively. The effect of [Eth] on mRNA transcription is assumed to follow Michaelis-Menten kinetics (Eq. 4) to describe its saturation behaviour when ethylene binds to the receptor. Finally, the concentrations of nucleotides to produce mRNA in Eq. 4 and amino acids to produce ACS in Eq. 5 are assumed to be constant and absorbed into $k_{RNA,syn}$ and $k_{ACS,syn}$, respectively.

For ACO dynamics, the decrease in its activity mainly downregulates post-climacteric ethylene biosynthesis (Van de Poel et al., 2012). Therefore, to emphasise the post-climacteric stage and reduce the model complexity, we focused on modelling the degradation of ACO to amino acids only, downregulating ethylene biosynthesis with time (Eq. 1 and Eq. 6). We did not model the biosynthesis of ACO as our experimental data in the preclimacteric stage were not sufficiently informative to infer any model assumption. ACO can thus be viewed as a ripeness indicator of the fruit - the lower the ACO, the riper the fruit.

$$\frac{d}{dt}[\mathrm{ACO}] = -k_{\mathrm{ACO,deg}}[\mathrm{ACO}][\mathrm{Eth}] \tag{6}$$

where $k_{ACO,deg}$ is a rate constant (m^3 $mol^{-1}s^{-1}$) of the ACO degradation to amino acid.

The output of the ethylene model is the exchange rate of ethylene to the environment, which is calculated by

$$\varphi_{\mathrm{Eth}} = -\frac{k_{\mathrm{d,Eth}}}{\rho_{\mathrm{p}}}([\mathrm{Eth}]_{\infty} - [\mathrm{Eth}]) \tag{7}$$

with φ_{Eth} being the exchange rate of ethylene (mol $kg^{-1}s^{-1}$) and ρ_p is pear density (kg m^{-3}). During storage and shelf-life, $[Eth]_\infty$ is considered 0 mol m^{-3}.

2.1.3. Dynamics of respiration rate

The respiration model usually starts from a quasi-steady state Michaelis-Menten-based model (Hertog et al., 1998). Furthermore, since our experiment was conducted at a low and constant CO_2 level, no CO_2 inhibition was applied to the Michaelis-Menten-based model. Next, by incorporating diffusion of O_2 and CO_2 through pear skin, the exchange rate of these respiratory gases can be written below, which is also referred to as the static model of respiration, as explained in Section 2.1.2.

$$\frac{d}{dt}[\mathrm{O_2}] = -\frac{R_{\mathrm{O_2,\,max}}[\mathrm{O_2}]}{K_{\mathrm{m,O_2}} + [\mathrm{O_2}]} + k_{\mathrm{d,O_2}}([\mathrm{O_2}]_{\infty} - [\mathrm{O_2}]) \tag{8}$$

$$\frac{d}{dt}[\mathrm{CO_2}] = r_{\mathrm{q,ox}}R_{\mathrm{O_2}} + \frac{R_{\mathrm{CO_2,\,max,f}}}{1 + \frac{[\mathrm{O_2}]}{K_{\mathrm{m,CO_2,f}}}} + k_{\mathrm{d,CO_2}}([\mathrm{CO_2}]_{\infty} - [\mathrm{CO_2}]) \tag{9}$$

where $R_{O2,max}$ and $R_{CO2,max,f}$ are the maximum rate of O_2 consumption (mol $m^{-3}s^{-1}$) and fermentative CO_2 production, respectively; $K_{m,O2}$ and $K_{m,CO2,f}$ are Michaelis-Menten constants (mol m^{-3}) for oxidative respiration rate and fermentation, respectively; $r_{q,ox}$ is the respiration quotient of oxidative respiration, and $R_{O_2} = \frac{R_{O_2,\,max}[O_2]}{K_{m,O_2}+[O_2]}$is the O_2 consumption rate (mol $m^{-3}s^{-1}$), referred to as a source term in Eq. 8. The overall diffusion constants ($k_{d,O2}$ and $k_{d,CO2}$, s^{-1}) describe the diffusion rate of O_2 and CO_2 through the skin, respectively, which are calculated as Eq. 3 with the skin permeability coefficient of the corresponding gases. Furthermore, since in Fig. 1, the ethylene biosynthesis also consumes O_2 and produces CO_2, Eqs. 8 and 9 were added with the ethylene production term as below.

$$\frac{d}{dt}[\mathrm{O_2}] = -\frac{R_{\mathrm{O_2,\,max}}[\mathrm{O_2}]}{K_{\mathrm{m,O_2}} + [\mathrm{O_2}]} - \frac{R_{\mathrm{Eth,\,max}}[\mathrm{O_2}]}{K_{\mathrm{m,Eth}} + [\mathrm{O_2}]} + k_{\mathrm{d,O_2}}([\mathrm{O_2}]_{\infty} - [\mathrm{O_2}]) \tag{10}$$

$$\frac{d}{dt}[\mathrm{CO_2}] = r_{\mathrm{q,ox}}R_{\mathrm{O_2}} + \frac{R_{\mathrm{CO_2,\,max,f}}}{1 + \frac{[\mathrm{O_2}]}{K_{\mathrm{m,CO_2,f}}}} + \frac{R_{\mathrm{Eth,\,max}}[\mathrm{O_2}]}{K_{\mathrm{m,Eth}} + [\mathrm{O_2}]} + k_{\mathrm{d,CO_2}}([\mathrm{CO_2}]_{\infty} - [\mathrm{CO_2}]) \tag{11}$$

Since the dynamic respiration, viewed by CO_2 production, comprises oxidative respiration and fermentation, it is complex to model the whole process. Therefore, this paper mainly focuses on the dynamic change in oxidative respiration while assuming that fermentation is time-independent, only depending on the O_2 level. The maximum rate of O_2 consumption can be expressed as:

$$R_{\mathrm{O_2,\,max}} = k_{\mathrm{rsp}}[\mathrm{E}] \tag{12}$$

where k_{rsp} is a rate constant (s^{-1}) from an enzyme-substrate complex to a product following the Michaelis-Menten enzymatic reaction scheme for a single enzyme (Cornish-Bowden, 1979). [E] is the respiration enzyme concentration (mol m^{-3}).

Due to fruit ripening, the respiration enzyme can be produced or degraded over time, which drives the changes in respiration. In this study, we assumed that internal ethylene regulates the production of the respiratory enzyme (Fig. 1). The change in [E] can be written as below.

$$\frac{d}{dt}[\mathrm{E}] = k_{\mathrm{E,syn}}[\mathrm{Eth}] - k_{\mathrm{E,deg}}[\mathrm{E}] \tag{13}$$

where $k_{E,syn}$ and $k_{E,deg}$ are rate constants (s^{-1}) of production and degradation of the single respiratory enzyme [E], respectively.

In line with the assumption underlying the Michaelis-Menten equation, we assumed that the enzyme concentration changes result in a rapid adaptation of the respiration enzyme-substrate complex, establishing a quasi-steady state again.

Finally, the model outputs are the exchange rate of O_2 and CO_2, which are calculated as follows.

$$\varphi_{\mathrm{O_2}} = \frac{k_{\mathrm{d,O_2}}}{\rho_{\mathrm{p}}}([\mathrm{O_2}]_{\infty} - [\mathrm{O_2}]) \tag{14}$$

$$\varphi_{\mathrm{CO_2}} = \frac{k_{\mathrm{d,CO_2}}}{\rho_{\mathrm{p}}}([\mathrm{CO_2}] - [\mathrm{CO_2}]_{\infty}) \tag{15}$$

with φ_X being the exchange rate of gas X (mol $kg^{-1}s^{-1}$) referring to either O_2 or CO_2, and ρ_p is pear density (kg m^{-3}).

2.1.4. Temperature dependence of kinetic rate constants

The effect of temperature on rate constants k of enzymatic reactions and maximum rates (R_{max}) in the Michaelis-Menten equations mentioned in Sections 2.1.2 and 2.1.3 is modelled by Arrhenius's law.

$$k(T) = k_{\mathrm{ref}}\exp\left(-\frac{E_{\mathrm{a}}}{R}\left(\frac{1}{T} - \frac{1}{T_{\mathrm{ref}}}\right)\right) \tag{16}$$

where k and k_{ref} are the rate constant at temperature T (K) and the rate constant at a reference temperature T_{ref} (assigned at 283.15 K), respectively; E_a is the activation energy (J mol^{-1}); R is the ideal gas constant (J $mol^{-1}K^{-1}$).

2.2. Fruit and storage experiment

'Conference' pears (*Pyrus communis*) were harvested in the commercial harvesting window (on 05/09/2023) from a commercial orchard in Bierbeek, Belgium (COBB). After being transported to the Flanders Centre of Postharvest Technology, Belgium (VCBT), the fruit was randomised and precooled at −1 °C in regular air (RA) for 21 d. After the cold-conditioning, the pears were randomly divided into three batches. The first batch (approximately 50 kg of pears) was immediately exposed for 14 d to shelf-life condition (18 °C, RA) with respiration and ethylene exchange rate being measured every 2 d. Each measurement

day, 10 new fruit were used. This shelf-life dataset, measured after cold conditioning, is referred to as the harvest data.

Of the remaining two batches, one (approximately 630 kg of pears) was used for the lab-scale storage at VCBT, while the other (approximately 180 kg of pears) was returned to COBB for industrial-scale storage. After each storage period, fruit were transferred to shelf-life condition (18 °C, RA) for approximately 12–18 h before the first shelf-life measurements were carried out. During these measurements, 7 fruit were used per sampling day.

Regarding the lab-scale storage at the VCBT, rigid polypropylene containers (dimension: 0.715 m × 0.515 m × 0.965 m, thickness: 5 mm) were used to implement different CA and DCA conditions. The containers were equipped with a water lock to ensure gas-tightness and connected to an in-house built controller, monitoring gas condition using an optical O_2 sensor (FDO2, Pyroscience, Germany) and a non-dispersive infrared (NDIR) type CO_2 sensor (ExplorIR-W, SST Sensing, UK).

Five different CA conditions were implemented in the lab-scale storage experiment:

- CAP41 (4 °C, 1 kPa O_2, 0.7 kPa CO_2),
- CAP45 (4 °C, 5 kPa O_2, 0.7 kPa CO_2),
- CAN11 (-1 °C, 1 kPa O_2, 0.7 kPa CO_2),
- CAN15 (-1 °C, 5 kPa O_2, 0.7 kPa CO_2), and
- CAN13 (-1 °C, 3 kPa O_2, 0.7 kPa CO_2)

For DCA, two containers were stored at −1 °C in the lab-scale storage experiment:

- DCA4M31, maintained DCA conditions for four months, after which it was operated under CA conditions (2 months at 3 kPa O_2 followed by 1 month at 1 kPa O_2)
- DCA8M, maintained DCA conditions for eight months.

For both DCA containers, RQ-DCA was employed with an RQ threshold of 1.3, and the frequency of RQ determination was once every 11 h, with the measurement itself taking around 5 h. The RQ-DCA only controlled the O_2 set point level in the containers while keeping the CO_2 level at 0.7 kPa. More details on the DCA controller algorithm are provided by Bessemans et al. (2016). Since RQ was determined by the controller through in situ respiration measurements, the data on respiration rate during storage are available for these containers. Fig. 2 illustrates the timeline for the different batches of pears taken out of storage containers for a shelf-life measurement and a practical trajectory of a storage condition at the industry scale.

2.3. Michaelis-Menten experiment

This experiment was used to measure respiration and ethylene exchange rates at various combinations of O_2 and temperature, thereby calibrating the static Michaelis-Menten part of the developed models. In this experiment, the pears at harvest, the pears from DCA4M31 (February 2024), the pears from COBB (March 2024), and the pears from DCA8M (June 2024) were used. It should be noted that at harvest for ethylene measurement, only the fruit at 18 °C in regular air gave reliable results, while the measurement results from the other conditions were below the detection limit. For logistical reasons, pears taken out from DCA4M31 (February 2024), COBB (March 2024), and DCA8M (June 2024) were first stored for two weeks at −1 °C in 3 kPa O_2 before being used for the Michaelis-Menten experiment. The experiment conditions are marked in Fig. 3, where each combination consists of 5 replicate fruit.

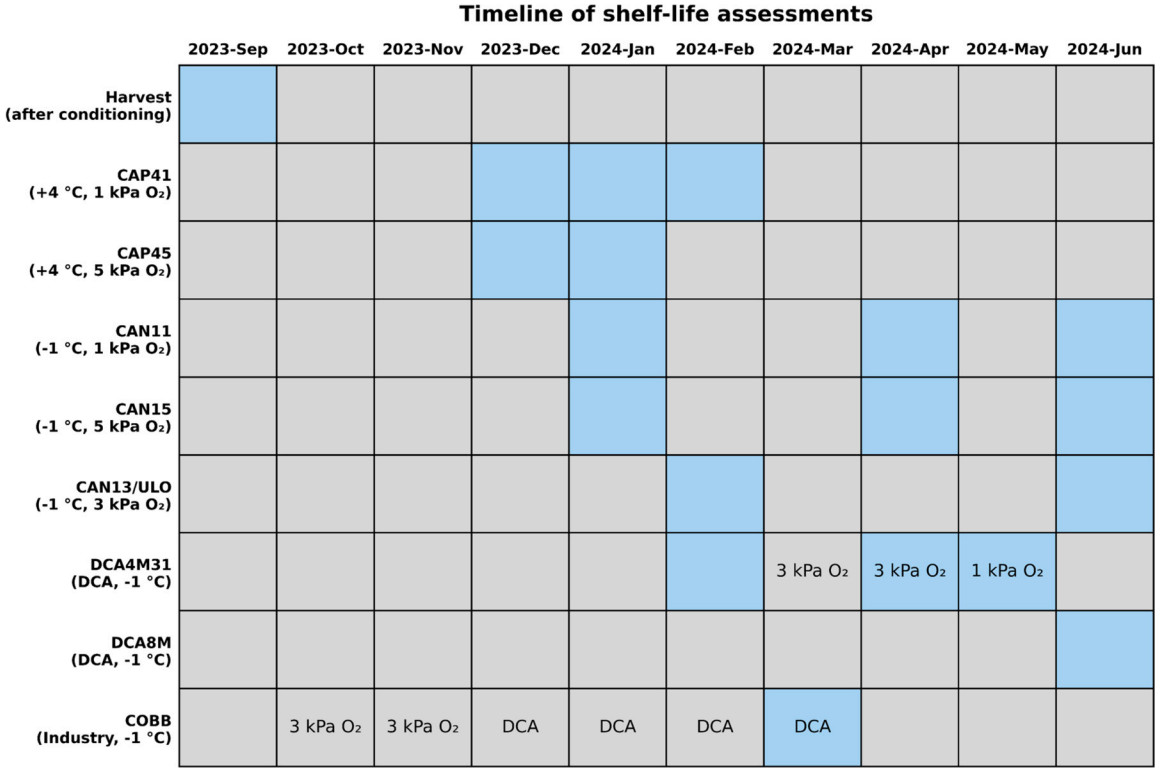

Fig. 2. A timeline of 'Conference' pear taken out of storage conditions, under varying temperature and O_2 level (with CO_2 level fixed at 0.7 kPa), for shelf-life measurement. Blue cells indicate when the pears were taken out of storage settings. The container DCA4M31 was opened in February 2024 to take a sample of pears out, and then was operated under CA conditions with different O_2 levels (kPa) mentioned in each cell. The COBB-industry scale storage followed a practical storage trajectory, switching after 2 months from CA at 3 kPa O_2 to DCA.

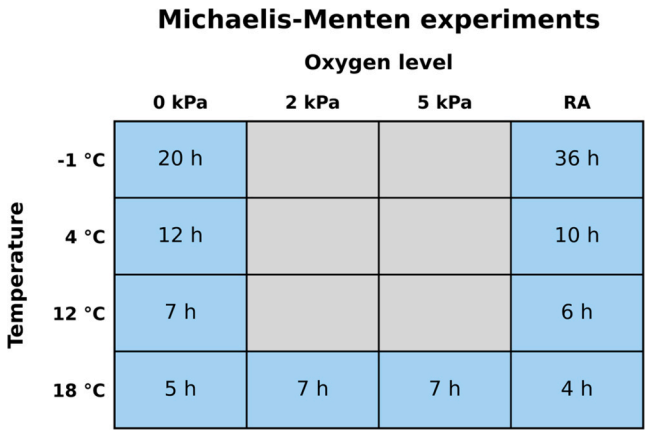

Fig. 3. A combination of oxygen and temperature (blue cells) for the Michaelis-Menten experiment to measure respiration and ethylene exchange rates (RA: regular air). The value in each blue cell indicates the period (h) between two measurements for gas exchange rates.

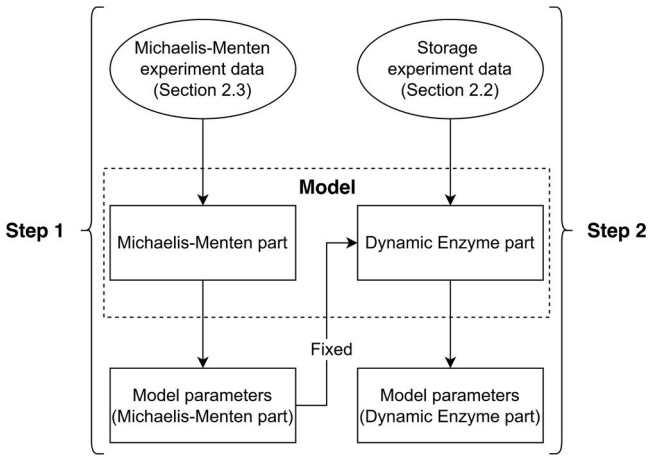

Fig. 4. A two-step procedure for model calibration for the dynamic model integrating ethylene biosynthesis and respiration. The coupled model of ethylene biosynthesis and respiration consists of two parameter groups: parameters associated with the Michaelis-Menten formulation and parameters governing the enzyme dynamics. In step 1, Michaelis-Menten experiment data (Section 2.3) were used to calibrate the parameter set from the Michaelis-Menten formulation in the dynamic model, which was subsequently kept fixed. In step 2, the storage experiment data (Section 2.2) were used to calibrate the model parameters of the dynamic enzyme part of the coupled model.

2.4. Respiration and ethylene measurement

Measurement of respiration and ethylene exchange rates in shelf-life assessments and Michaelis-Menten experiments followed the protocols described in Ho et al. (2018) and Bulens et al. (2011), respectively. In this study, respiration and ethylene exchange rates were measured on the same individual fruit.

Individual pears were weighed and placed in air-tight jars of 1.7 L that were flushed with the specified gas conditions at the specified temperatures for 36–40 h to allow the fruit to adapt to the imposed conditions. After this flushing period, the jars were closed, and the initial gas composition inside the jars was measured: ethylene (in ppm) by CompactGC (Interscience, Louvain-la-Neuve, Belgium) and respiratory gases, O_2 and CO_2 (in %), by a gas analyser (CheckMate II, PBI, Dansensor, Denmark). The jars were kept for a certain period under the specified conditions before the second measurement was conducted. The exact period depended on the condition studied (See Fig. 3). To convert the ethylene (ppm) and respiratory gases (%) to gas moles, temperature, free volume of the jar, and jar pressure were used with the ideal gas law. Finally, the gas exchange rates of O_2, CO_2, and ethylene were calculated from the change in the gas concentration in the jar during the experiment. For example,

$$\varphi_{O_2} = \frac{n_{O_2,1} - n_{O_2,2}}{m_p \Delta t} \tag{17}$$

Where φ_{O2} is exchange rate of O_2 (mol $kg^{-1}s^{-1}$); $n_{O_2,1}$ and $n_{O_2,2}$ are the moles of O_2 at the first and second measurements, calculated by the ideal gas law; Δt is the waiting time (s) between two measurements; m_p is the pear mass (kg).

2.5. Datasets and parameter estimation

The models were calibrated through a two-step approach (Fig. 4). First, the Michaelis-Menten submodels in the static ethylene and respiration models were calibrated using the Michaelis-Menten dataset in Section 2.3 to obtain $R_{max,Eth,harvest,ref}$, $E_{a,Eth}$, $K_{m,Eth}$, $R_{O2,max,harvest,ref}$, $E_{a,O2}$, $K_{m,O2}$, $R_{CO2,max,f,ref}$, $E_{a,CO2}$, and $K_{m,CO2,f}$. Second, the enzyme turnover submodels of ethylene biosynthesis and respiration were calibrated with the shelf-life datasets (including harvest after cold-conditioning, CAP41, CAP45, CAN11, CAN15, and DCA4M31) and the measured respiration data during the storage period of DCA4M31. Finally, the remaining three shelf-life datasets, CAN13, DCA8M, and COBB, were used to validate the model since these are conditions with practical relevance. Model calibration and validation were mainly carried out in OptiPa, an in-house developed MATLAB-based software (Hertog et al., 2007).

The models of ethylene biosynthesis and respiration are highly nonlinear, involving many parameters and unmeasured state variables, such as mRNA and enzyme levels. A normalisation technique was employed to set the initial value of unmeasured state variables to 1. As a consequence of this normalisation, the units of certain parameters will be changed because they are now lumped with the enzyme concentrations (Table 2). More details about the normalisation can be found in the supplementary data, with section S1 for the ethylene model and section S2 for the respiration model. Finally, some parameters were either obtained from the literature or fixed during the calibration routine to reduce the complexity and overcome the high correlation with other parameters. Parameters obtained from the literature and fixed after pre-optimisation are shown in Table 3.

Table 2
A list of normalised variables, including states and parameters, and their mathematical expression after normalisation.

Variables	Normalised variables	Mathematical expression
Ethylene model		
[mRNA]	[mRNA]*	$[\text{mRNA}]^* = \frac{[\text{mRNA}]}{[\text{mRNA}]_{t=0}}$
[ACS]	[ACS]*	$[\text{ACS}]^* = \frac{[\text{ACS}]}{[\text{ACS}]_{t=0}}$
[ACO]	[ACO]	$[\text{ACO}]^* = \frac{[\text{ACO}]}{[\text{ACO}]_{t=0}}$
$k_{RNA,syn}$	$k^*_{RNA,syn}$	$k^*_{RNA,syn} = \frac{k_{RNA,syn}}{[\text{mRNA}_{ACS}]_{t=0}}$
$k_{ACS,syn}$	$k^*_{ACS,syn}$	$k^*_{ACS,syn} = k_{ACS,syn}\frac{[\text{mRNA}_{ACS}]_{t=0}}{[\text{ACS}]_{t=0}}$
k_{Eth}	k^*_{Eth}	$k^*_{Eth} = k_{Eth}[\text{ACS}]_{t=0}[\text{ACO}]_{t=0}$
Respiration model		
[E]	[E]*	$[\text{E}]^* = \frac{[\text{E}]}{[\text{E}]_{t=0}}$
$k_{E,syn}$	$k^*_{E,syn}$	$k^*_{E,syn} = \frac{k_{E,syn}}{[\text{E}]_{t=0}}$
k_{rsp}	k^*_{rsp}	$k^*_{rsp} = k_{rsp}[\text{E}]_{t=0}$

Table 3
Parameters from the literature and the fixed-parameter assumption for the dynamic model of ethylene biosynthesis and respiration.

Parameter	Value	Unit	Reference
Common parameter			
P_{O2}	6.74×10^{-7}	m s^{-1}	(Ho et al., 2018)
P_{CO2}	10.2×10^{-7}	m s^{-1}	(Ho et al., 2018)
A_P/V_P	93.30	m^{-1}	(Rogge et al., 2015)
Ethylene model			
$E_{a,RNA,deg}$	0	kJ mol^{-1}	After pre-optimization
$E_{a,ACS,syn}$	14	kJ mol^{-1}	After pre-optimization
Respiration model			
$E_{a,E,deg}$	400	kJ mol^{-1}	After pre-optimization

3. Results

3.1. Parameters of Michaelis-Menten models

The measured data from the Michaelis-Menten experiment (Section 2.3) were used to calibrate the static models of the O_2, CO_2 and ethylene exchange rates of the pear fruit, considering different time points separately with maximum rates $R_{Eth,max}$ and $R_{O2,max}$ for each set of data from the Harvest (after three-week conditioning), DCA4M31 (February 2024), DCA8M (June 2024), and COBB (March 2024) experiments. Other Michaelis-Menten parameters were considered as generic parameters unaffected by time. The adjusted coefficients of determination (R^2_{adj}) were 0.91 for O_2, 0.87 for CO_2, and 0.77 for ethylene. Additionally, a good alignment of the simulated exchange rates of three gases from the static models with the corresponding measured values was also shown in Figure S1 (supplementary data).

All estimated parameters for the static models are shown in Table 4. For the static ethylene model, the maximum production rate of ethylene ($R_{Eth,max,ref}$) at harvest was 0.82 ± 0.11 nmol $m^{-3}s^{-1}$, which is significantly lower than that after several storage months. The $R_{Eth,max,ref}$ values after four months and eight months in DCA (DCA4M31 and DCA8M) were 116.7 ± 7.2 nmol $m^{-3}s^{-1}$ and 116.2 ± 7.2 nmol $m^{-3}s^{-1}$, respectively, while $R_{Eth,max,ref}$ after five months in the industry condition (COBB) was the highest with 315 ± 10 nmol $m^{-3}s^{-1}$. The estimated maximum consumption rate of O_2 in the static respiration model showed a similar pattern to the static ethylene model. The maximum consumption rate of O_2 ($R_{O2,max}$) at harvest was the lowest, while $R_{O2,max}$ after 5 months in the industry condition was the highest. After 4 months and 8 months in DCA storage, the values of $R_{O2,max}$ were similar, around 59 µmol $m^{-3}s^{-1}$. Finally, the CO_2 production rate by fermentation ($R_{CO2,max,f}$) was 47.82 ± 0.78 µmol $m^{-3}s^{-1}$, which is considered a common parameter, as our assumption in Section 2.1.3.

Table 4
Parameters of static models of ethylene biosynthesis and respiration in 'Conference' pear. The maximum production/consumption rate is referred to at the reference temperature of 10 °C. The reported value represents the mean and standard error of the estimated parameters.

Parameter	Value	Unit
Ethylene		
$R_{Eth,max,harvest,ref}$ (k^*_{Eth})[1]	0.82 ± 0.11	nmol $m^{-3}s^{-1}$
$R_{Eth,max,DCA4M31,ref}$	116.7 ± 7.2	nmol $m^{-3}s^{-1}$
$R_{Eth,max,DCA8M,ref}$	116.2 ± 7.2	nmol $m^{-3}s^{-1}$
$R_{Eth,max,COBB,ref}$	315 ± 10	nmol $m^{-3}s^{-1}$
$E_{a,Eth}$	79.9 ± 2.4	kJ mol^{-1}
$K_{m,Eth}$	204 ± 32	mmol m^{-3}
Respiration		
$R_{O2,max,harvest,ref}$ (k^*_{rsp})[2]	47.1 ± 1.6	µmol $m^{-3}s^{-1}$
$R_{O2,max,DCA4M31,ref}$	59.6 ± 1.7	µmol $m^{-3}s^{-1}$
$R_{O2,max,DCA8M,ref}$	58.5 ± 1.7	µmol $m^{-3}s^{-1}$
$R_{O2,max,COBB,ref}$	85.1 ± 2.1	µmol $m^{-3}s^{-1}$
$E_{a,O2}$	90.6 ± 1.3	kJ mol^{-1}
$K_{m,O2}$	184 ± 48	mmol m^{-3}
$R_{CO2,max,f,ref}$	47.82 ± 0.78	µmol $m^{-3}s^{-1}$
$E_{a,CO2}$	58.9 ± 1.3	kJ mol^{-1}
$K_{m,CO2,f}$	4.6 ± 2.0	mmol m^{-3}
$r^{[3]}_{q,ox}$	1	

[1] and [2] $R_{Eth,max,harvest,ref}$ and $R_{O2,max,harvest,ref}$ were proved in the supplementary data to be k^*_{Eth} and k^*_{rsp} used in the dynamic model of ethylene biosynthesis and respiration, respectively. Noted that k^*_{Eth} and k^*_{rsp} were normalised parameters of k_{Eth} and k_{rsp}, respectively, after the normalisation process mentioned in Section 2.5.

[3] $r_{q,ox}$ is kept fixed at 1, following Lammertyn et al. (2003) when estimating all parameters in the static respiration model.

3.2. Changes of fermentation metabolism during storage

Although fermentation was treated as time-independent in our model development, this section estimated separately $R_{CO2,max,f,ref}$ to assess changes of the fermentation metabolism at harvest, after four and eight months in DCA (DCA4M31 and DCA8M), and after five months in an industry condition (COBB). The result is shown in Table 5, indicating $R_{CO2,max,f,ref}$ changes after harvest, depending on time and storage conditions. Specifically, the $R_{CO2,max,f,ref}$ decreased after four and eight months in DCA, compared to harvest.

3.3. Parameters of enzyme turnover models

The coupled model consists of ethylene and respiration submodels, including enzyme turnover, which, together, were calibrated and validated as described in Section 2.5. The parameter estimation of the coupled model is shown in Table 6. Furthermore, the sensitivity analysis and correlation matrix of estimated parameters are displayed in Figure S2 and Table S1 of the supplementary data, respectively. Most of the estimated parameters had a relative standard error less than 30%, except for the $k^*_{RNA,syn,ref}$ with 35.4%, still moderately acceptable (Table 6). The sensitivity analysis showed that the model outputs are sensitive to most of the estimated parameters. Regarding the correlation matrix, all of the parameter pairs showed a correlation coefficient (R) below a correlation threshold ($|R| \leq 0.9$).

The coupled model could explain 68% of the overall variation in the calibration dataset (R^2_{adj} of 0.68), explaining 50% and 85% of the variation for ethylene and respiration, respectively. Finally, the mean absolute percentage error (MAPE) was around 33% when the coupled model was evaluated with the validation set. Furthermore, MAPE and root mean square error (RMSE) for our model prediction at each shelf-life assessment after different storage conditions are also displayed in Table S2 (Supplementary data). In general, the actual values of MAPE and RMSE for each shelf-life assessment are acceptably low and close to the ideal values of MAPE and RMSE, which represent the minimum errors that the ideal model can achieve. More details about the model behaviour for both ethylene and respiration during storage and shelf life are described in the next sections.

Table 5
Maximum CO_2 production rate of 'Conference' pear by fermentation ($R_{CO2,max,f,ref}$) at harvest, after four-month DCA (DCA4M31), after eight-month DCA (DCA8M), and after five months in industry storage (COBB). The reference temperature is at 10 °C. The reported value represents the mean and standard error of the estimated parameters.

Parameter	Value	Unit
$R_{CO2,max,f,harvest,ref}$	53.6 ± 1.5	µmol $m^{-3}s^{-1}$
$R_{CO2,max,f,DCA4M31,ref}$	41.2 ± 1.3	µmol $m^{-3}s^{-1}$
$R_{CO2,max,f,DCA8M,ref}$	37.3 ± 1.1	µmol $m^{-3}s^{-1}$
$R_{CO2,max,f,COBB,ref}$	58.7 ± 1.1	µmol $m^{-3}s^{-1}$

Table 6
Estimated parameters for enzyme dynamics in the coupled model describing both ethylene biosynthesis and respiration. The estimated parameters are reported in mean ± standard error (θ ± SE), and the relative standard error (RSE) is calculated as $RSE = \frac{SE}{|\theta|} \times 100\%$. The reference temperature of rate constants was set at 10 °C.

Parameter	Value	Unit	RSE
Ethylene			
$k^*_{RNA,syn,ref}$	9.6 ± 3.4	d^{-1}	35.4
$k_{RNA,deg,ref}$	0.180 ± 0.032	d^{-1}	17.8
$E_{a,RNA,syn}$	52.8 ± 5.2	kJ mol^{-1}	9.8
$K_{m,RNA}$	7.5 ± 1.6	mmol m^{-3}	21.3
$k^*_{ACS,syn,ref}$	8.1 ± 1.3	d^{-1}	16.0
$k_{ACS,deg,ref}$	0.071 ± 0.011	d^{-1}	15.5
$E_{a,ACS,deg}$	68.2 ± 7.4	kJ mol^{-1}	10.9
$k_{ACO,deg,ref}$	16.37 ± 0.97	m^3 $mol^{-1}d^{-1}$	5.9
$E_{a,ACO,deg}$	76.4 ± 3.0	kJ mol^{-1}	3.9
Respiration			
$k^*_{E,syn,ref}$	13.41 ± 0.67	m^3 $mol^{-1}d^{-1}$	5.0
$k_{E,deg,ref}$	$5.34 \times 10^{-4} \pm 0.62 \times 10^{-4}$	d^{-1}	11.6
$E_{a,E,syn}$	117.00 ± 5.02	kJ mol^{-1}	4.3
$r_{q,ox}$ [a]	0.9611 ± 0.0099	-	1.0

[a] $r_{q,ox}$ was re-estimated together with the other parameters of enzyme kinetics for respiration.

3.4. Calibration and validation of the coupled model of ethylene biosynthesis and respiration

The coupled model of ethylene biosynthesis and respiration was calibrated and validated with the measurement data as described in Section 2.5. The output of the model is presented separately in Section 3.4.1 for the dynamics of ethylene biosynthesis and Section 3.4.2 for the dynamics of respiration rate.

3.4.1. Dynamics of ethylene biosynthesis

The measured and simulated results for the calibration and validation datasets are shown in Fig. 5 and Fig. 6, respectively. Both figures have the same harvest plot from the calibration dataset to easily compare the change throughout storage. Generally, the calibration results aligned well with the measurements for the ethylene exchange rate in shelf-life. However, the simulation of ethylene exchange rate at harvest and during shelf-life assessment after CA storage at 4 °C in 5 kPa O_2 (CAP45) still showed a mismatch with measurement data (Fig. 5 and Table S2). Next, two observations should be emphasised. First, the earlier the pears were taken out, the later the climacteric peak was reached, as indicated by the timing of the increase in ethylene exchange rate. Second, by looking at CA storage at both 4 °C and −1 °C in 1 kPa O2 (Fig. 5 B1–3 and Fig. 5 D1–3, respectively), and CA storage at −1 °C in both 1 kPa and 5 kPa O_2 (Fig. 5 D1–3 and Fig. 5 E1–3), it can be seen that the higher the temperature and/or O_2 level in storage, the earlier the climacteric peak comes. Interestingly, the validation in Fig. 6 shows that the ethylene model can predict the difference in ethylene exchange rate after eight months between CA storage at −1 °C in 3 kPa O_2 (Fig. 6 B2) and DCA storage at −1 °C (Fig. 6 C). It can be clearly seen that after eight months of storage, the fruit stored at −1 °C in 3 kPa O_2 came to the full ripe stage as the ethylene emission rate decreased, while the fruit from DCA at −1 °C had a similar behaviour to the ethylene emission rate at harvest (after cold conditioning). Finally, the model also predicted well the pattern of the ethylene exchange rate of pears after five months of industrial storage (Fig. 6 D).

3.4.2. Dynamics of respiration rate

The measured data of the exchange rate of O_2 and CO_2 showed a similar pattern, and the model prediction generally matched the measured data in shelf-life. Therefore, only the results of the O_2 exchange rate are selected to represent the respiration model in shelf-life. First, the calibration dataset and the modelled respiration data are visualised in Fig. 7. The figure begins with the harvest plot to easily compare the change throughout storage. The experimental data reveal a general pattern of the O_2 exchange rate during the subsequent shelf-life periods after different storage conditions from harvest. At harvest, the exchange rate of O_2 has a long lag phase (around 4 d), while the rates during the subsequent shelf-life periods increase steadily to level off at approximately 300 - 400 nmol $kg^{-1}s^{-1}$ after one week in shelf-life. At the end of the shelf-life, the measured exchange rate of O_2 seems to be decreasing. The simulated results acceptably match the measured data, except for the last 4 d of shelf-life. During these days, the measured rates slightly decrease while the simulation still shows an increasing trend in respiration. This deviation can be most clearly observed for the condition at + 4 °C in 1 kPa O_2 (Fig. 7 B1) and the condition at −1 °C and 5 kPa O_2 (Fig. 7 E3).

Fig. 8 shows the measured and simulated O_2 exchange rate for the validation conditions, i.e., CA storage at −1 °C in 3 kPa (Fig. 8 B1–2), DCA storage at −1 °C after 8 months (Fig. 8 C), and an industrial storage (Fig. 8 D). Similar to Fig. 7, Fig. 8 also starts with the plot at harvest from the calibration set to easily compare the change in the gas exchange rates in shelf-life after storage periods. The model could capture the dynamic change in respiration rate of pears in CA storage at −1 °C in 3 kPa O_2 (CAN13) and in the industry condition (COBB). Especially for the first week in shelf-life, the model prediction follows the validation dataset well. However, the respiration model under-predicted the O_2 exchange rate of pears at DCA at −1 °C (DCA8M). Furthermore, the mismatched decrease in respiration from day 8 in shelf-life was also observed, but this downtrend was only shown for a few storage periods. However, in general, the model could predict the general behaviour of the O_2 exchange rate in shelf-life after a long-term storage period in different conditions from CA to DCA, and from laboratory scale to industry scale.

Fig. 9 shows the measured and simulated results of the exchange rates of respiratory gases for DCA storage in four months (DCA4M31) as calibration and for DCA storage in eight months (DCA8M) as validation. It can be seen that the model prediction aligned quite well with the measurement. Specifically, the simulated O_2 rate matched the measured rate for both datasets. However, there was a small offset between the simulated and measured CO_2 rate during two storage periods.

3.5. Simulation of the coupled model

The validated model was used to simulate gas exchange rates of pears during storage periods to gain insight into their physiological response under different conditions.

Fig. 10 shows the simulation of the ethylene submodel to show the simulated model behaviour during the actual storage periods, either for eight months of CA storage at −1 °C in 3 kPa O_2 (CAN13) or DCA at −1 °C (DCA8M), and during five months of the industrial condition (COBB). As compared to CA storage at −1 °C in 3 kPa O_2 (CAN13), the ethylene exchange rate was suppressed during DCA storage in the O_2 regime below 1 kPa, while the ethylene exchange rate in CA storage at −1 °C in 3 kPa O_2 increased and reached its climacteric peak during storage after five months. The evolution of mRNA and ACS also followed the dynamic pattern of the ethylene exchange rate in each condition. Furthermore, the simulation suggests that the ACO of pears from CA at −1 °C in 3 kPa O_2 degraded faster than that from DCA at −1 °C. For the pears in the industrial storage (COBB), it can be seen from the O_2 levels that at first, the storage condition was at −1 °C under 3 kPa O_2 for two months, and then the O_2 level was reduced by a DCA system to around 1.5 kPa during the last three months. Although DCA storage was applied for the last three months, the exchange rate of ethylene still increased during storage, compared to the DCA at −1 °C (DCA8M) in the laboratory scale. The content of ACS and its mRNA in COBB was also higher than that in DCA8M.

Finally, the simulations of the O_2 exchange rate during storage

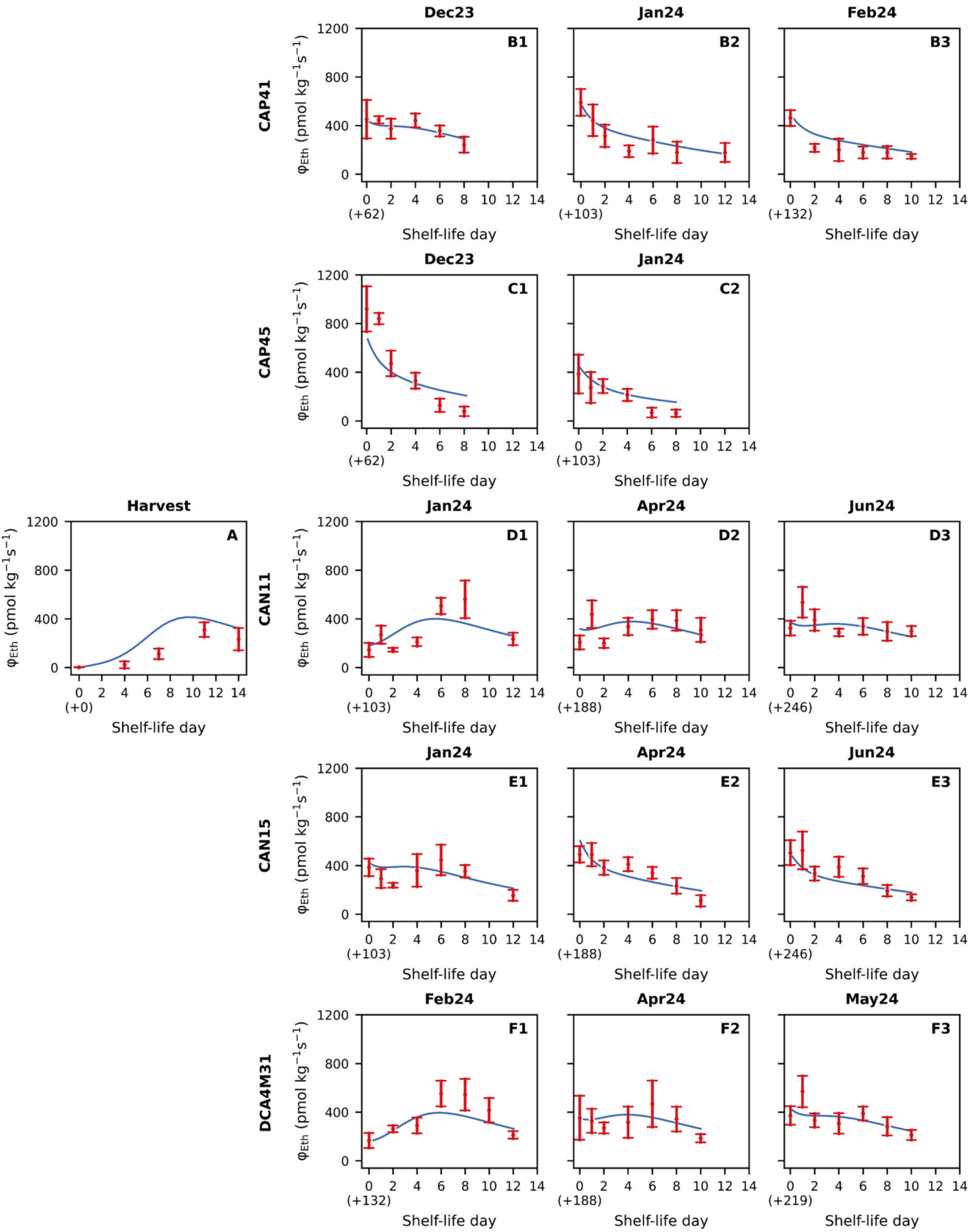

Fig. 5. Calibration dataset of ethylene exchange rate (φ_{Eth}) in shelf-life (18 °C in regular air) after several months in CA storage at 4 °C in 1 kPa O_2 (CAP41) and 5 kPa O_2 (CAP45), and CA storage at −1 °C in 1 kPa O_2 (CAN11) and 5 kPa O_2 (CAN15), and DCA storage at −1 °C (DCA4M31) in DCA condition (until February 2024), then changed to 3 kPa O_2 (until April 2024) then 1 kPa O_2 (until May 2024). The experiment day after storage was indicated as (+ day). Scatter points represent experimental data with their mean ± standard deviation, while solid lines represent the simulated results.

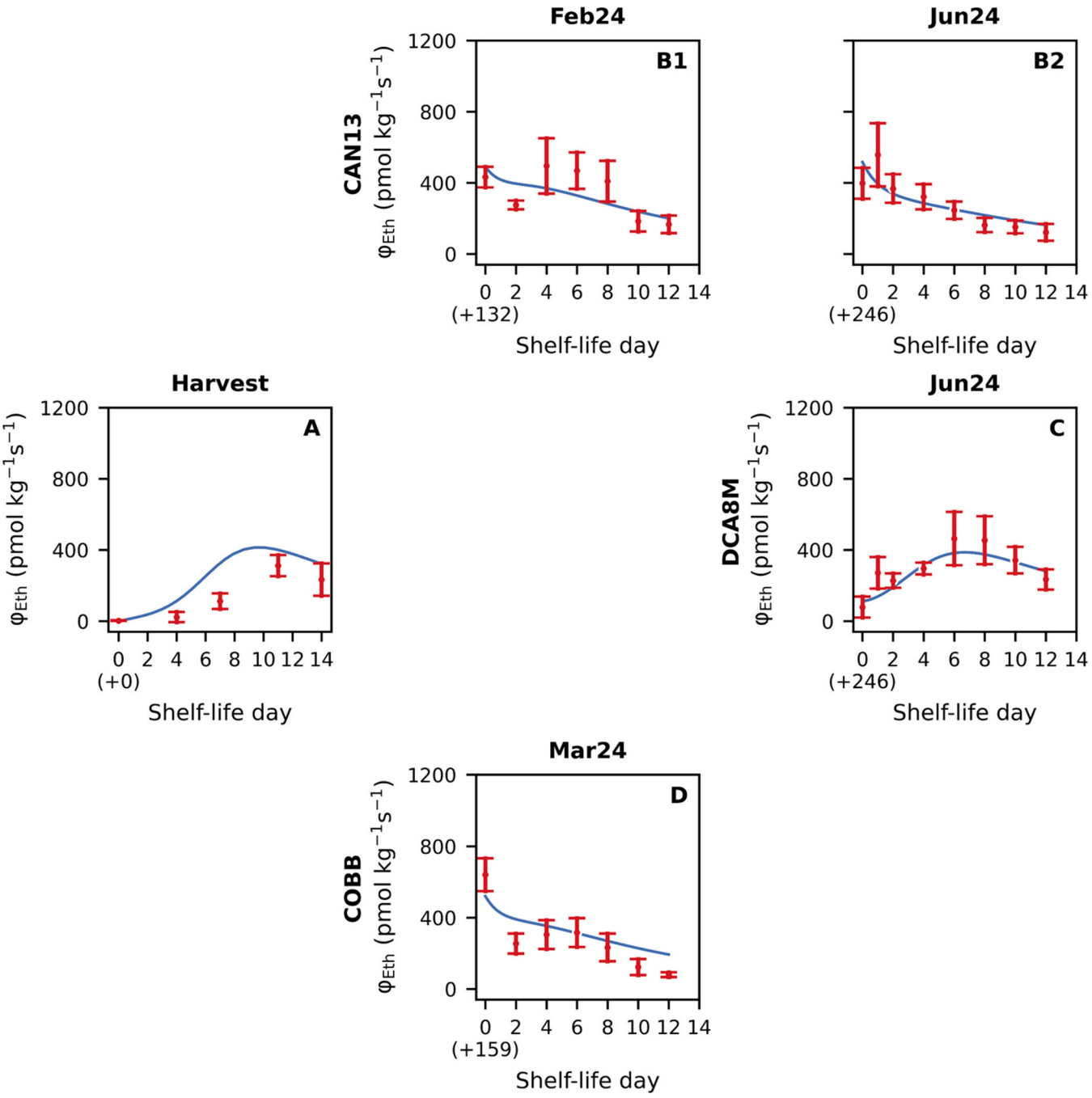

Fig. 6. Validation dataset of ethylene exchange rate (φ_{Eth}) in shelf-life (18 °C in regular air) after several months in CA storage at −1 °C in 3 kPa O_2 (CAN13), DCA storage at −1 °C (DCA8M) for 8 months, and in an industrial storage condition (COBB). The experiment day after storage was indicated as (+ day). Scatter points represent the mean ± standard deviation of the experimental data, while solid lines represent the simulated results. The harvest data were not part of the validation data but were provided for reference.

periods are shown in Fig. 11 for CA storage at −1 °C in 3 kPa O_2 (CAN13), DCA storage at −1 °C (DCA8M), and an industrial condition (COBB), to compare the respiration evolution during storage. It can be seen that the O_2 exchange rate dropped and stayed stable for the whole storage period when the O_2 level decreased to below 1 kPa. In contrast, the exchange rate of O_2 in CA storage at −1 °C and 3 kPa O_2 increased over time. Furthermore, similar to the ethylene exchange rate, the O_2 exchange rate in the industrial condition (COBB) was also higher and increased slowly, compared with that in the DCA condition (DCA8M).

4. Discussion

4.1. R_{max} drives the temporal changes in ethylene and respiration

Calibration of the static model for ethylene and respiration in Table 4 revealed that the maximum rates of ethylene production ($R_{Eth,max}$) and O_2 consumption ($R_{O2,max}$) changed after several months of storage. These estimated values of $R_{i,max}$ and activation energy ($E_{a,i}$) in the static models were comparable to values determined in other studies (Ho et al., 2018; Verreydt et al., 2022). Generally, the maximum rates of ethylene production and O_2 consumption increased after long-term storage from harvest. $R_{Eth,max}$ and $R_{O2,max}$ can be related to enzyme

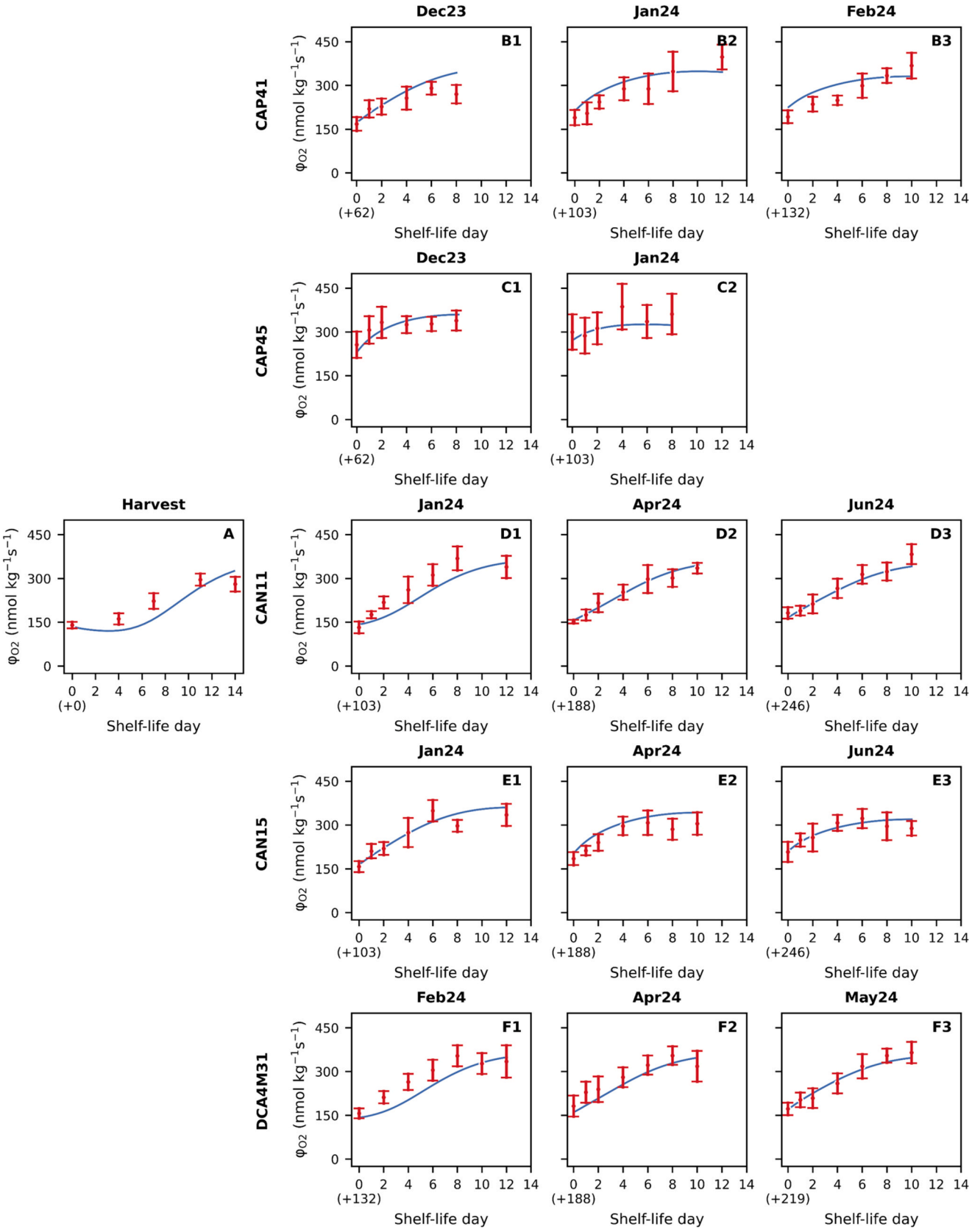

Fig. 7. Calibration dataset of O_2 exchange rate (φ_{O2}) in shelf-life (18 °C in regular air) after several months in CA storage at 4 °C in 1 kPa O_2 (CAP41) and 5 kPa O_2 (CAP45), and CA storage at −1 °C in 1 kPa O_2 (CAN11) and 5 kPa O_2 (CAN15), and DCA storage at −1 °C (DCA4M31) in DCA condition (until February 2024), then changed to 3 kPa O_2 (February-April 2024) then 1 kPa O_2 (April-May 2024). The experiment day after storage was indicated as (+ day). Scatter points represent experimental data with their mean ± standard deviation, while solid lines represent the simulated results.

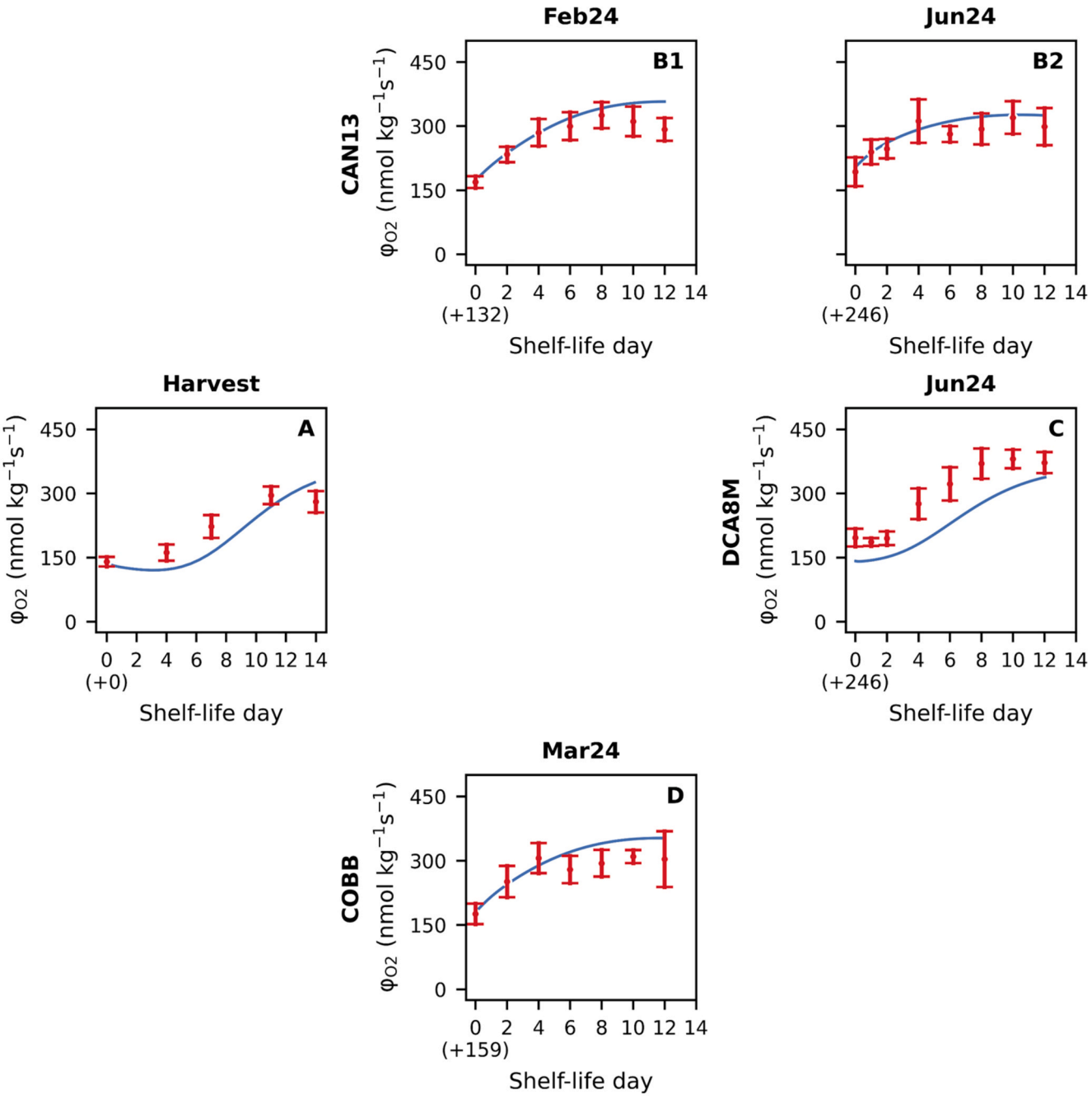

Fig. 8. Validation dataset of O_2 exchange rate (φ_{O2}) in shelf-life (18 °C in regular air) after several months in CA storage at −1 °C in 3 kPa O_2 (CAN13), DCA storage at −1 °C (DCA8M) for 8 months, and in industrial storage conditions (COBB). The experiment day after storage was indicated as (+ day). Scatter points represent experimental data with their mean ± standard deviation, while solid lines represent the simulated results. The harvest data were not part of the validation data but were provided for reference.

activities involved in ethylene biosynthesis and respiration. Several experimental studies have observed something similar. It is reported that the increase in ACS and ACO activity, together with upregulation of the corresponding gene expressions for 'Conference' pear during and after storage (Chiriboga et al., 2012, 2013). For respiration, a recent study showed that the transcription level of alternative oxidase (AOX) has been observed to increase during tomato ripening (Iglesias-Sanchez et al., 2025). These results support our modelling hypothesis that the $R_{Eth,max}$ and $R_{O2,max}$ should dynamically change over time to be able to describe the evolution of ethylene biosynthesis and respiration during storage and shelf life, likely due to climacteric ripening

Regarding fermentation, Table 5 shows that after long-term storage in DCA at extremely low O_2, $R_{CO2,max,f}$ decreases. Boeckx et al. (2019a) also observed a decrease in fermentation of apples in their study when the apples were exposed to prolonged low O_2 stress. They hypothesised that there was a switch to an alternative pathway, such as alanine instead of ethanol fermentation, to reduce carbon losses (Boeckx et al., 2019b). However, as only DCA storage (Fig. 2) and a few experimental conditions (Fig. 3) could potentially trigger fermentation, we decided to treat fermentation as time-independent to reduce the complexity of the coupled model.

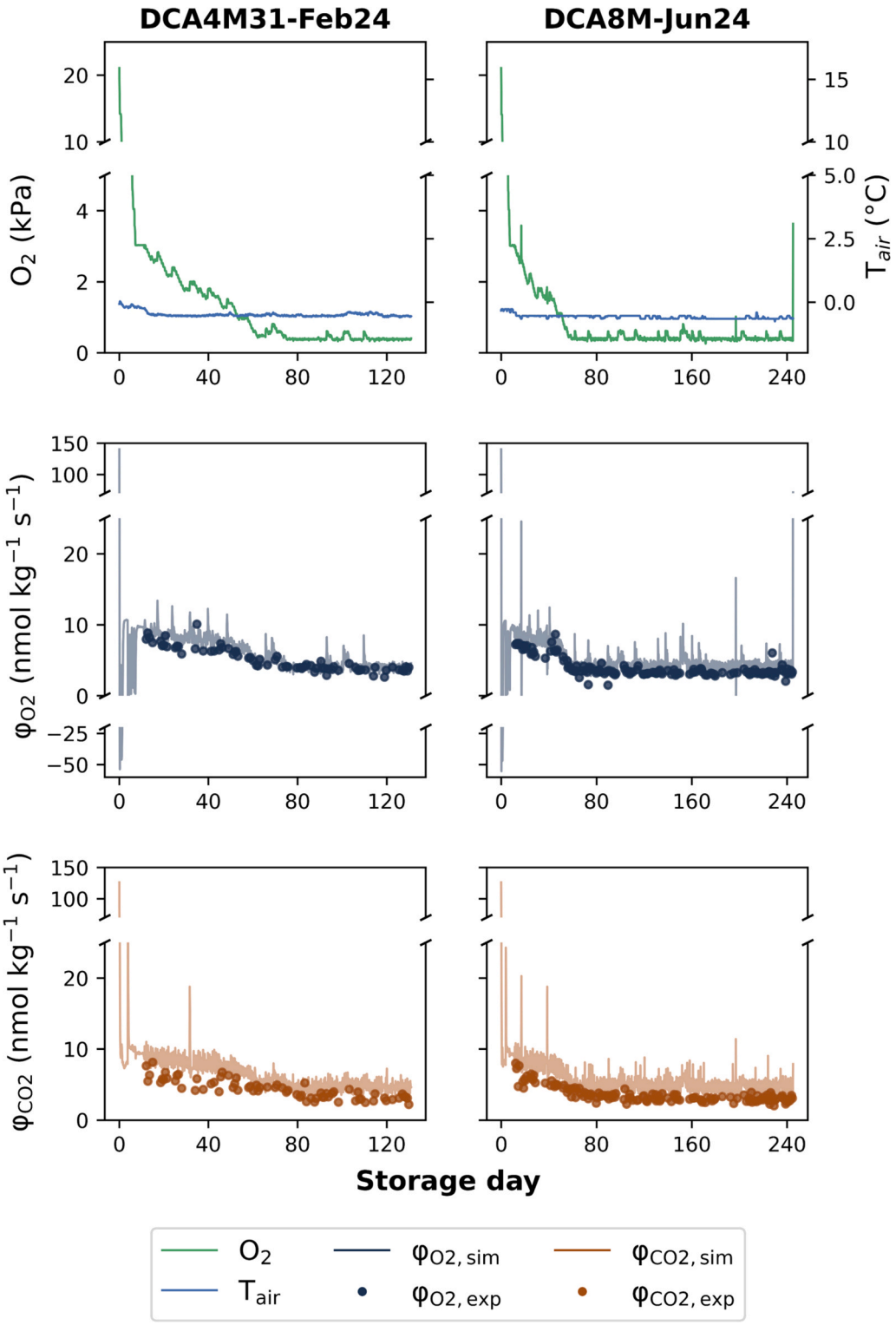

Fig. 9. Exchange rate of O_2 and CO_2 during storage in DCA at −1 °C after 4 months (DCA4M31) for calibration and in DCA at −1 °C after 8 months (DCA8M) for validation. Each storage condition (O_2 and temperature) is displayed in the first row. The scatter points represent the experimental data, while the solid lines represent the simulated results for the exchange rates.

4.2. The coupled model well captures the overall dynamics of ethylene biosynthesis and respiration

The coupled model was developed starting from the known mechanisms of ethylene biosynthesis and respiration, with some simplification. Despite the considerable biological variance in the measurement data, the model prediction was acceptably accurate enough ($R^2_{adj,\ calibration}$ of 0.68) to describe different practical storage conditions, spanning from laboratory scale to industry scale.

Furthermore, the correlation coefficient of parameter pairs (|R|) was always less than 0.9. Therefore, no severe pairwise parameter correlation was observed. This threshold is commonly used to determine strong

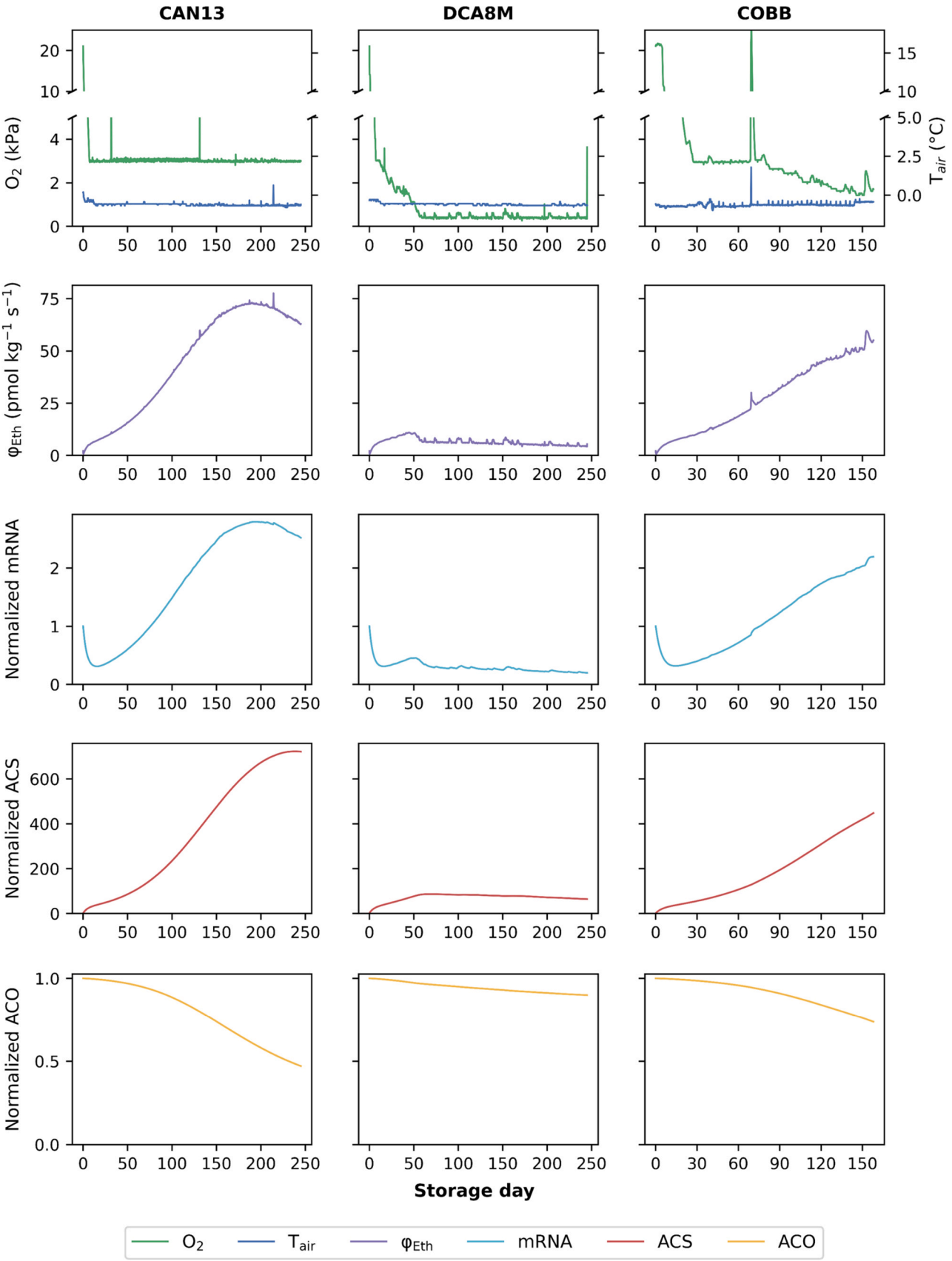

Fig. 10. Simulation result of ethylene biosynthesis model during storage at different storage conditions: CA storage at −1 °C in 3 kPa O_2 (CAN13 until June 2024), DCA at −1 °C for 8 months (DCA8M), and industrial storage (COBB).

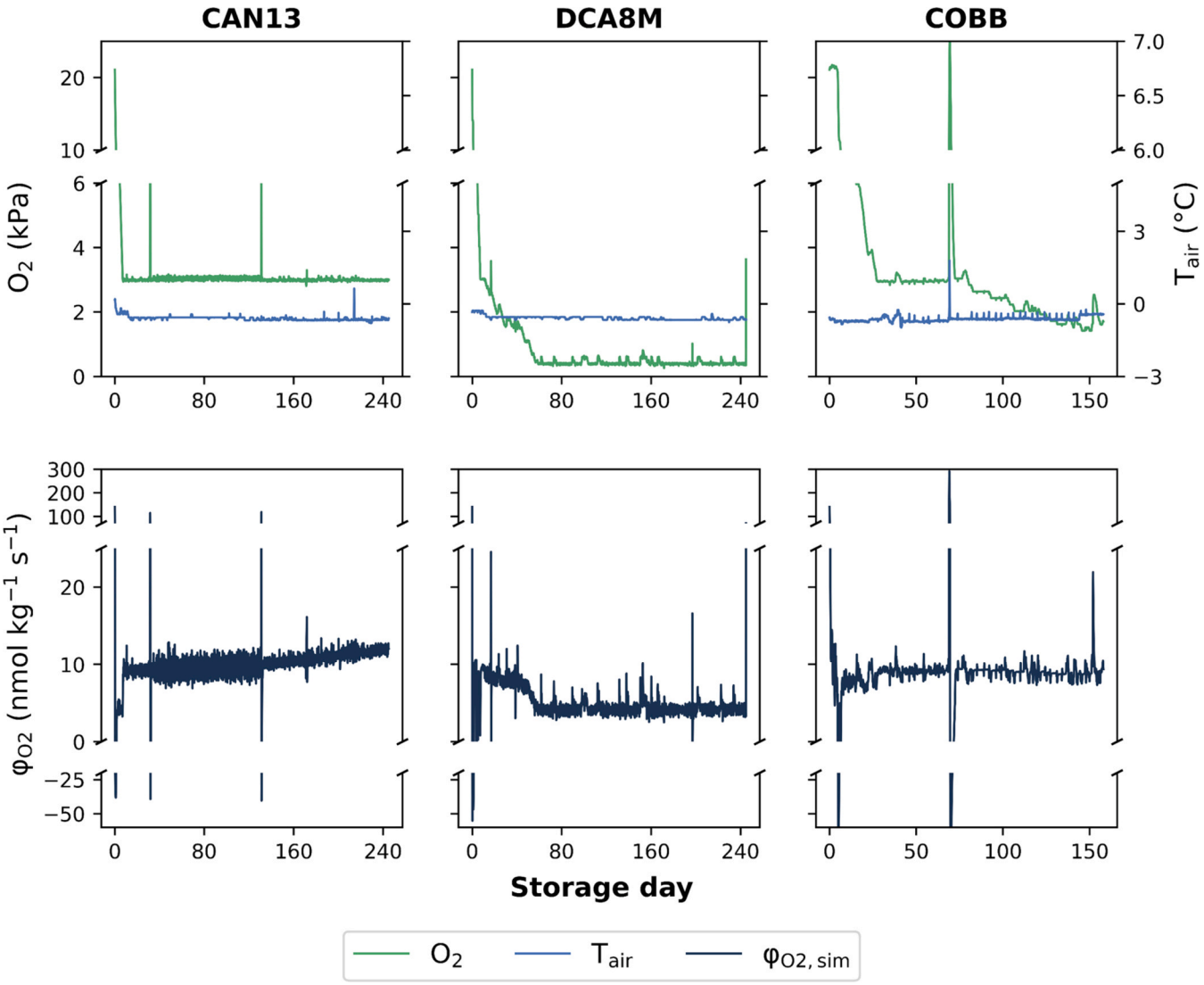

Fig. 11. Simulation result of O_2 exchange rate during storage at different storage conditions: CA storage at −1 °C in 3 kPa O_2 (CAN13 until June 2024), DCA at −1 °C for 8 months (DCA8M), and an industrial condition (COBB).

parameter dependency (Brun et al., 2001; Saucedo et al., 2024). Furthermore, the relative standard error of estimated parameters was also acceptably low (< 36%). Next, a sensitivity matrix was established to assess the local structural identifiability. The rank of the sensitivity matrix is full, indicating that our model structure is at least locally identifiable (Joubert et al., 2020).

The model predicted well the processes of ethylene biosynthesis and respiration during shelf-life. The general trend of the ethylene exchange rate (Fig. 5 and Fig. 6) increasing and subsequently decreasing has been observed in different studies (Wang et al., 1972; Chen et al., 1993; Hiwasa et al., 2003; Johnston et al., 2009; Villalobos-Acuña et al., 2011; Chiriboga et al., 2013; Saquet and Streif, 2017), while the increase in the exchange rate of respiratory gases during shelf-life after storage (Fig. 7 and Fig. 8) has also been reported previously for several European pear cultivars (Saquet and Streif, 2017; Saquet and Almeida, 2017; Brandes and Zude-Sasse, 2019). Interestingly, the exchange rate of ethylene and O_2 did not strictly proportionally evolve during shelf-life. This suggests that the relation between these exchange rates is governed by underlying metabolic processes, rather than a direct coupling between the two rates. Furthermore, the model has the ability to predict the respiration rate during DCA storage, validated from the measurement (Fig. 9). Additionally, it can be seen in Fig. 9 and Fig. 11 that the simulated O_2 exchange rate during storage showed some peaks and/or negative values. This behaviour can be attributed to the abrupt changes in the O_2 profile, particularly at the start of (D)CA storage, or when the container was opened for shelf-life assessments. Such events caused a temporary significant difference between $[O_2]$ and $[O_2]_\infty$, resulting in peaks or even outward (thus, negative) instead of inward oxygen fluxes when $[O_2]_\infty$ dropped rapidly below $[O_2]$. Finally, it should be noted that during our model development, we assumed that the ethylene concentration outside the fruit was approximately zero due to the fact that during shelf-life measurement, the shelf-life room air was always ventilated. This assumption was also applied during the storage period because the ethylene concentration in the container was not available in our measurement system.

4.3. *A trade-off between simplicity and model performance is necessary*

For the ethylene model, the main noticeable deviation in prediction comes from the shelf-life measurement at harvest, where the ethylene model overpredicts the exchange rate of ethylene, compared to the measurement data (Fig. 5). This mismatch is expected to result from the model assumptions since we mainly focused on the autocatalytic ethylene biosynthesis process. It is speculated that the fruit may still be

using system 1 ethylene biosynthesis, resulting in an extended lag phase in the ethylene emission rate, even after 21 d of cold conditioning at harvest. Furthermore, according to studies from Lindo-García et al. (2020a, 2020b), ethylene biosynthesis is not only regulated by the enzyme system itself but also by other hormones such as gibberellins, salicylic acid, and jasmonic acid. At harvest, the amount of these hormones is usually high, which inhibits ethylene production. During the precooling period, these hormones will decrease. However, in this study, only the ethylene exchange rate was measured, which makes it challenging to interpret the underlying processes. For this, more measurements should be conducted at the hormone and proteomic levels (Tipu and Sherif, 2024).

Regarding the respiration model, the mismatch was observed in the decrease of respiration from day 8 of shelf-life (Fig. 8 B1). It can be attributed to the inconsistent behaviour of the respiration rate in the calibration data set (Fig. 7). Particularly, the measured respiration rate in the calibration set only showed a downward trend for a few storage periods. Furthermore, in Fig. 8, there was an underprediction of the O_2 exchange rate from DCA at −1 °C after 8 months (DCA8M). It may be hypothesised that the fruit might be more metabolically active than expected at high temperature (18 °C) and a high O_2 level (21 kPa) after a very long time at low O_2 (0.4 kPa). However, more rigorous studies focusing specifically on the enzyme turnover are needed to confirm this hypothesis.

Next, there was a small but consistent overprediction of the CO_2 exchange rate during storage (DCA4M31 and DCA8M) in Fig. 9. We speculate that this discrepancy results from three sources. First, the respiration model limited itself to modelling the dynamic changes in the oxidative respiration process associated with enzyme turnover, while keeping fermentation as a time-independent process. Boeckx et al. (2019a) developed a kinetic model of the fermentation process of apple at low O_2 storage conditions, which successfully captured the fermentation dynamics. Hence, the model performance could possibly be improved by also including the kinetics of the fermentative respiration. However, this will require more data under fermentation-inducing storage conditions, which was not the intention in this work. Second, the produced CO_2 from respiration at the cellular level could be associated with H_2O to form HCO_3^- and H^+ through the carbonic acid equilibrium, which reduces the CO_2 released to the headspace. This is supported by a study of Bessemans et al. (2020), where the equilibrium of CO_2 in water was added to their respiration model at the cellular level, which showed a good model performance of the respiration model under CA storage for pears. Third, the permeability coefficient of respiratory gases through pear skin was obtained from Ho et al. (2018), instead of being directly measured, which could contribute to the mismatch in the model output of CO_2. However, the current data were not rich enough to extend the model for these aspects.

4.4. DCA is beneficial compared to CA storage

It is interesting to note that in Table 4, the maximum rates of ethylene production ($R_{Eth,max}$) and O_2 consumption ($R_{O2,max}$) after 4 months in DCA (DCA4M31) were higher than those at harvest, while these rates after 4 months in DCA (DCA4M31) were comparable to those after 8 months in DCA (DCA8M). Based on the O_2 concentration during the DCA regime below 1 kPa (Fig. 9), it revealed that during the ultra-low O_2 regime in DCA storage, respiration and ethylene rates could be suppressed and evolved very slowly during storage. These findings are supported by the model predictions, shown in Fig. 10 for ethylene (simulation) and Fig. 9 for respiration (measurement and simulation).

Next, the simulation in Fig. 11 shows that the respiration rate of 'Conference' pear increased over time in CA storage at −1 °C in 3 kPa O_2 (CAN13), while the rate evolved very slowly and was maintained at a lower level in DCA at −1 °C (DCA8M). Additionally, the magnitude of the respiration rate in CA storage at −1 °C in 3 kPa O_2 (CAN13) was also higher than that in DCA storage at −1 °C (DCA8M). Thewes et al. (2020) and Wendt et al. (2024) also came to the same finding for the lower respiration in DCA than in CA conditions, for apple and pear, respectively. It highlights the benefits of DCA over CA in storage management since respiration heat from fruit substantially contributes to energy use in the cooling plant. Several studies reported that DCA could save 10 - 20% of energy use, compared to CA storage (Kittemann et al., 2015; Verlinden et al., 2023; Phan et al., 2026b).

Specifically to ethylene, this gaseous hormone is usually linked with the ripening response to quality deterioration during storage and shelf-life (Barry and Giovannoni, 2007; Tucker et al., 2017). The simulation of ethylene and its enzyme kinetics during the storage period in Fig. 10 revealed that the ethylene exchange rate continues to increase during CA storage at −1 °C in 3 kPa O_2 (CAN13), while the rate was slowed down and maintained at a lower level for DCA at −1 °C (DCA8M). This pattern was also observed for mRNA and ACS during the storage period between CAN13 and DCA8M. Furthermore, the simulated change of mRNA and ACS during CA storage (Fig. 10) is in line with a finding of Bulens (2012) who reported the increased ACS activity of 'Jonagold' apple during CA storage. Next, as explained in Section 2.1.2, ACO can be viewed as a ripening indicator in the model, where the lower ACO content refers to more ripe fruit. Therefore, based on their ACO content during both storage and shelf-life, the fruit stored in CA at −1 °C in 3 kPa O_2 (CAN13) were more ripe than those in DCA at −1 °C (DCA8M). This is also supported by the measured exchange rates of ethylene and respiratory gases during shelf-life (Fig. 6 and Fig. 8, respectively). Particularly, the ethylene-based climacteric peak for pears from DCA at −1 °C was only reached after 6 d in shelf-life, while pears from CA at −1 °C in 3 kPa O_2 already passed this peak after 1 d in shelf-life. The O_2 exchange rate in shelf-life for pear from DCA at −1 °C was also higher than those from CA at −1 °C in 3 kPa O_2. Therefore, this confirmed that during shelf-life, pears from the DCA condition are more retarded in their ripening process than those from the CA condition after long-term storage, which should possibly result in better quality retention during shelf-life (Bessemans et al., 2016).

4.5. Early application of DCA maximises its beneficial effects

From calibration of the static models (Table 4), the $R_{Eth,max}$ and $R_{O2,max}$ after 5 months of industrial storage (COBB) were the highest, compared to DCA at −1 °C after 4 months (DCA4M31) and after 8 months (DCA8M). The simulation from the coupled model for ethylene in Fig. 10 and for respiration in Fig. 11 also showed that these gas exchange rates in the industry condition (COBB) were higher than for DCA at −1 °C but less than for CA at −1 °C in 3 kPa O_2 (CAN13). This is plausible since the industrial storage condition from Fig. 11 started with CA conditions (3 kPa O_2) before being switched to a DCA condition. It should be noted that commercial cold rooms are prone to gas leakage (Bessemans et al., 2018), which also makes it challenging to achieve an O_2 level lower than 1.5 kPa O_2 during DCA. As a result, the ethylene exchange rate slowed down but did not significantly decrease in the DCA regime for the industrial storage (Fig. 10). A similar pattern was also observed for the respiration simulation (Fig. 11). Due to the initial CA storage period, ethylene biosynthesis has already been triggered, making it more challenging to suppress this ethylene biosynthesis and respiration during the subsequent DCA period. Therefore, we recommend DCA to be implemented without delay to maximise its benefits.

4.6. Towards an industrial implementation

Despite the model being a simplified representation of the underlying metabolic mechanisms, the model structure is still too complex to be implemented in practice as such. The sensitivity analysis can reveal the parameter importance, which would help practitioners prioritise which parameters should be accurately estimated in model implementation (Zi, 2011). The sensitivity result (Section S4) showed that $k^*_{RNA,syn,ref}$,

K_{RNA}, $k^*_{ACS,syn,ref}$, $k_{ACO,deg,ref}$, and $k^*_{E,syn,ref}$ had big impacts on the model outputs, so they should be prioritised for accurate estimation in practical applications. These parameters are associated with essential processes, i.e., the transcription process of RNA_{ACS}, the ACS production, ACO degradation, and a respiratory enzyme (E), which could be referred to as AOX (discussed in Section 4.1). Although $r_{q,ox}$ and some activation energies also showed high impacts on the model output, these are typically considered fixed enzyme properties which can be easily estimated from dedicated datasets. Finally, less sensitive parameters can be simply reused to reduce the calibration burden.

5. Conclusions

A coupled dynamic respiration and ethylene biosynthesis model was developed, going beyond the traditional Michaelis-Menten framework. The idea was to integrate a reaction framework to describe the change in the corresponding enzymes, which influence the maximum O_2 consumption rate ($R_{O2,max}$) and the maximum ethylene production rate ($R_{Eth,max}$) in the Michaelis-Menten model of respiration and ethylene biosynthesis, respectively. The coupled model was calibrated and validated using relevant practical storage conditions for 'Conference' pear under both laboratory and industry settings. Due to the experimental focus on gas exchange rates, the reaction framework of enzyme turnover had to be simplified. Despite limitations due to this simplification, the results still showed that the model simulations generally agree well with the measured data. Based on the calibrated model, several insights were obtained. First, DCA can suppress respiration and ethylene biosynthesis during storage better than CA, which can potentially maintain quality and save energy better for long-term storage. Second, at an extremely low O_2 level (0.5 kPa O_2) due to the DCA, the pear fruit seemingly adapts to the hypoxic condition, which significantly suppresses respiration and ethylene biosynthesis. Finally, DCA conditions should be implemented from the start of the storage period to maximise the benefits from DCA technology.

CRediT authorship contribution statement

Hoang Minh Phan: Writing – review & editing, Writing – original draft, Visualization, Methodology, Investigation, Formal analysis, Conceptualization. **Bart M. Nicolaï:** Writing – review & editing, Supervision, Funding acquisition, Conceptualization. **Maarten L.A.T.M Hertog:** Writing – review & editing, Conceptualization. **Pieter Verboven:** Writing – review & editing, Funding acquisition, Conceptualization. **Bert E. Verlinden:** Writing – review & editing, Conceptualization.

Declaration of Competing Interest

The authors declare that they have no known competing financial interests or personal relationships that could have appeared to influence the work reported in this paper.

Acknowledgements

This project has received funding from the European Union's Horizon 2020 research and innovation programme under grant agreement No 101036588, European food chain supply to reduce GHG emissions by 2050 (ENOUGH). The authors also acknowledge support of Flanders Innovation and Entrepreneurship (VLAIO ICON INFLEX HBC.2022.0677).

Appendix A. Supporting information

Supplementary data associated with this article can be found in the online version at doi:10.1016/j.postharvbio.2026.114675.

Data availability

Research Link Provided

Replication Data for: An integrated dynamic model of ethylene biosynthesis and respiration of 'Conference' pear (Pyrus communis) during storage and shelf life (KU Leuven RDR)

References

Alexander, L., Grierson, D., 2002. Ethylene biosynthesis and action in tomato: a model for climacteric fruit ripening. J. Exp. Bot. 53, 2039–2055. https://doi.org/10.1093/jxb/erf072.

Argueso, C.T., Hansen, M., Kieber, J.J., 2007. Regulation of ethylene biosynthesis. J. Plant. Growth Regul. 26, 92–105. https://doi.org/10.1007/s00344-007-0013-5.

Balci, H., Siper, M.C., Saleh, N., Safarli, I., Roy, L., Kilicarslan, M., Ozaydin, R., Mazein, A., Auffray, C., Babur, Ö., Demir, E., Dogrusoz, U., 2021. Newt: a comprehensive web-based tool for viewing, constructing and analyzing biological maps. Bioinformatics 37, 1475–1477. https://doi.org/10.1093/bioinformatics/btaa850.

Barbosa, N.C., Mendonça Vieira, R.A., De Resende, E.D., 2018. Modeling the respiration rate of Golden papayas stored under different atmosphere conditions at room temperature. Postharvest Biol. Technol. 136, 152–160. https://doi.org/10.1016/j.postharvbio.2017.11.005.

Barry, C.S., Giovannoni, J.J., 2007. Ethylene and fruit ripening. J. Plant. Growth Regul. 26, 143–159. https://doi.org/10.1007/S00344-007-9002-Y/FIGURES/2.

Bessemans, N., Verboven, P., Verlinden, B.E., Janssens, M., Hertog, M.L.A.T.M., Nicolaï, B.M., 2020. Apparent respiratory quotient observed in headspace of static respirometers underestimates cellular respiratory quotient of pear fruit. Postharvest Biol. Technol. 162, 111104. https://doi.org/10.1016/J.POSTHARVBIO.2019.111104.

Bessemans, N., Verboven, P., Verlinden, B.E., Nicolaï, B.M., 2018. Model based leak correction of real-time RQ measurement for dynamic controlled atmosphere storage. Postharvest Biol. Technol. 136, 31–41. https://doi.org/10.1016/j.postharvbio.2017.09.011.

Bessemans, N., Verboven, P., Verlinden, B.E., Nicolaï, B.M., 2016. A novel type of dynamic controlled atmosphere storage based on the respiratory quotient (RQ-DCA). Postharvest Biol. Technol. 115, 91–102. https://doi.org/10.1016/j.postharvbio.2015.12.019.

Binder, B.M., Jez, J.M., 2020. Ethylene signaling in plants. J. Biol. Chem. 295, 7710–7725. https://doi.org/10.1074/JBC.REV120.010854.

Boeckx, J., Hertog, M., Geeraerd, A., Nicolaï, B., 2019a. Regulation of the fermentative metabolism in apple fruit exposed to low-oxygen stress reveals a high flexibility. Postharvest Biol. Technol. 149, 118–128. https://doi.org/10.1016/j.postharvbio.2018.11.017.

Boeckx, J., Pols, S., Hertog, M.L.A.T.M., Nicolaï, B.M., 2019b. Regulation of the central carbon metabolism in apple fruit exposed to postharvest low-oxygen stress. Front. Plant. Sci. 10. https://doi.org/10.3389/fpls.2019.01384.

Brandes, N., Zude-Sasse, M., 2019. Respiratory patterns of European pear (Pyrus communis L. 'Conference') throughout pre- and post-harvest fruit development. Heliyon 5, e01160. https://doi.org/10.1016/J.HELIYON.2019.E01160.

Brun, R., Reichert, P., Künsch, H.R., 2001. Practical identifiability analysis of large environmental simulation models. Water Resour. Res. 37, 1015–1030. https://doi.org/10.1029/2000WR900350.

Bulens, I., 2012. Ethylene biosynthesis of "Jonagold" apple during storage and shelf life: a modeling approach. KU Leuven. Faculteit Bio-ingenieurswetenschappen, Leuven.

Bulens, I., Van de Poel, B., Hertog, M.L.A.T.M., Cristescu, S.M., Harren, F.J.M., De Proft, M.P., Geeraerd, A.H., Nicolaï, B.M., 2014. Dynamic changes of the ethylene biosynthesis in 'Jonagold' apple. Physiol. Plant. 150, 161–173. https://doi.org/10.1111/PPL.12084.

Bulens, I., Van de Poel, B., Hertog, M.L.A.T.M., De Proft, M.P., Geeraerd, A.H., Nicolaï, B.M., 2011. Protocol: an updated integrated methodology for analysis of metabolites and enzyme activities of ethylene biosynthesis. Plant. Methods 7. https://doi.org/10.1186/1746-4811-7-17.

Chang, C., 2016. Q&A: how do plants respond to ethylene and what is its importance? BMC Biol. 14 (1), 7. https://doi.org/10.1186/S12915-016-0230-0.

Chen, P.M., Varga, D.M., Mielke, E.A., 1993. Ripening behavior of `columbia' and `gebhard' strains of red `d'Anjou' pears after cold storage. J. Am. Soc. Hortic. Sci. 118, 81–85. https://doi.org/10.21273/JASHS.118.1.81.

Chiriboga, M.-A., Recasens, I., Schotsmans, W.C., Dupille, E., Larrigaudière, C., 2012. Cold-induced changes in ACC metabolism determine softening recovery in 1-MCP treated 'conference' pears. Postharvest Biol. Technol. 68, 78–85. https://doi.org/10.1016/j.postharvbio.2012.02.006.

Chiriboga, M.-A., Saladié, M., Giné Bordonaba, J., Recasens, I., Garcia-Mas, J., Larrigaudière, C., 2013. Effect of cold storage and 1-MCP treatment on ethylene perception, signalling and synthesis: influence on the development of the evergreen behaviour in 'Conference' pears. Postharvest Biol. Technol. 86, 212–220. https://doi.org/10.1016/j.postharvbio.2013.07.003.

Cornish-Bowden, A., 1979. Chapter 2 - Introduction to enzyme kinetics. In: Cornish-Bowden, A. (Ed.), Fundamentals of Enzyme Kinetics. Butterworth-Heinemann, pp. 16–38. https://doi.org/10.1016/B978-0-408-10617-7.50007-9.

De Wild, H.P.J., Woltering, E.J., Peppelenbos1, H.W., 1999. Carbon dioxide and 1-MCP inhibit ethylene production and respiration of pear fruit by different mechanisms. J. Exp. Bot. 50, 837–844. https://doi.org/10.1093/jxb/50.335.837.

Eccher Zerbini, P., 2002. The quality of pear fruit. In: Acta Horticulturae, pp. 805–810. https://doi.org/10.17660/ActaHortic.2002.596.139.

Fonseca, S.C., Oliveira, F.A.R., Brecht, J.K., 2002. Modelling respiration rate of fresh fruits and vegetables for modified atmosphere packages: a review. J. Food Eng. 52, 99–119. https://doi.org/10.1016/S0260-8774(01)00106-6.

Franck, C., Lammertyn, J., Ho, Q.T., Verboven, P., Verlinden, B., Nicolaï, B.M., 2007. Browning disorders in pear fruit. Postharvest Biol. Technol. 43, 1–13. https://doi.org/10.1016/j.postharvbio.2006.08.008.

Génard, M., Gouble, B., 2005. ETHY. A theory of fruit climacteric ethylene emission. Plant. Physiol. 139, 531. https://doi.org/10.1104/PP.105.063339.

Gwanpua, S.G., Verlinden, B.E., Hertog, M.L.A.T.M., Nicolaï, B.M., Geeraerd, A.H., 2017. A mechanistic modelling approach to understand 1-MCP inhibition of ethylene action and quality changes during ripening of apples. J. Sci. Food Agric. 97, 3802–3813. https://doi.org/10.1002/jsfa.8244.

Gwanpua, S.G., Vicent, V., Verlinden, B.E., Hertog, M.L.A.T.M., Nicolai, B.M., Geeraerd, A.H., 2014. Managing biological variation in skin background colour along the postharvest chain of "Jonagold" apples. Postharvest Biol. Technol. 93, 61–71. https://doi.org/10.1016/j.postharvbio.2014.02.008.

Hertog, M.L.A.T.M., Peppelenbos, H.W., Evelo, R.G., Tijskens, L.M.M., 1998. A dynamic and generic model of gas exchange of respiring produce: the effects of oxygen, carbon dioxide and temperature. Postharvest Biol. Technol. 14, 335–349. https://doi.org/10.1016/S0925-5214(98)00058-1.

Hertog, M.L.A.T.M., Verlinden, B.E., Lammertyn, J., Nicolaï, B.M., 2007. OptiPa, an essential primer to develop models in the postharvest area. Comput. Electron. Agric. 57, 99–106. https://doi.org/10.1016/j.compag.2007.02.001.

Hiwasa, K., Kinugasa, Y., Amano, S., Hashimoto, A., Nakano, R., Inaba, A., Kubo, Y., 2003. Ethylene is required for both the initiation and progression of softening in pear (Pyrus communis L.) fruit. J. Exp. Bot. 54, 771–779. https://doi.org/10.1093/jxb/erg073.

Ho, P.L., Tran, D.T., Hertog, M.L.A.T.M., Nicolaï, B.M., 2020. Modelling respiration rate of dragon fruit as a function of gas composition and temperature. Sci. Hortic. 263, 109138. https://doi.org/10.1016/j.scienta.2019.109138.

Ho, Q.T., Hertog, M.L.A.T.M., Verboven, P., Ambaw, A., Rogge, S., Verlinden, B.E., Nicolaï, B.M., 2018. Down-regulation of respiration in pear fruit depends on temperature. J. Exp. Bot. 69, 2049–2060. https://doi.org/10.1093/JXB/ERY031.

Ho, Q.T., Verboven, P., Verlinden, B.E., Lammertyn, J., Vandewalle, S., Nicolaï, B.M., 2008. A continuum model for metabolic gas exchange in pear fruit. PLOS Comput. Biol. 4, e1000023. https://doi.org/10.1371/JOURNAL.PCBI.1000023.

Ho, Q.T., Verboven, P., Verlinden, B.E., Schenk, A., Nicolaï, B.M., 2013. Controlled atmosphere storage may lead to local ATP deficiency in apple. Postharvest Biol. Technol. 78, 103–112. https://doi.org/10.1016/j.postharvbio.2012.12.014.

Iglesias-Sanchez, A., Del-Saz, N.F., Ezquerro, M., Feixes-Prats, E., Ribas-Carbo, M., Fernie, A.R., Rodriguez-Concepción, M., Florez-Sarasa, I., 2025. Activation of alternative oxidase ensures carbon supply for ethylene and carotenoid biosynthesis during tomato fruit ripening. https://doi.org/10.1101/2025.01.30.635696.

Jalali, A., Linke, M., Geyer, M., Mahajan, P.V., 2020. Shelf life prediction model for strawberry based on respiration and transpiration processes. Food Packag. Shelf Life 25. https://doi.org/10.1016/j.fpsl.2020.100525.

Johnston, J.W., Gunaseelan, K., Pidakala, P., Wang, M., Schaffer, R.J., 2009. Co-ordination of early and late ripening events in apples is regulated through differential sensitivities to ethylene. J. Exp. Bot. 60, 2689–2699. https://doi.org/10.1093/jxb/erp122.

Joubert, D., Stigter, J.D., Molenaar, J., 2020. An efficient procedure to assist in the re-parametrization of structurally unidentifiable models. Math. Biosci. 323, 108328. https://doi.org/10.1016/j.mbs.2020.108328.

Kappel, F., Fisher-Fleming, R., Hogue, E.J., 1995. Ideal Pear Sensory Attributes and Fruit Characteristics. HortSci 30, 988–993. https://doi.org/10.21273/HORTSCI.30.5.988.

Kittemann, D., McCormick, R., Neuwald, D.A., 2015. Effect of high temperature and 1-MCP application or dynamic controlled atmosphere on energy savings during apple storage. Eur. J. Hort. Sci. 80, 33–38. https://doi.org/10.17660/eJHS.2015/80.1.5.

Lakakul, R., Beaudry, R.M., Hernandez, R.J., 1999. Modeling respiration of apple slices in modified-atmosphere packages. J. Food Sci. 64, 105–110. https://doi.org/10.1111/j.1365-2621.1999.tb09870.x.

Lammertyn, J., Scheerlinck, N., Jancsók, P., Verlinden, B.E., Nicolaï, B.M., 2003. A respiration-diffusion model for "Conference" pears I: Model development and validation. Postharvest Biol. Technol. 30, 29–42. https://doi.org/10.1016/S0925-5214(03)00061-9.

Lindo-García, V., Larrigaudière, C., Duaigües, E., López, M.L., Echeverria, G., Giné-Bordonaba, J., 2020a. Elucidating the involvement of ethylene and oxidative stress during on- and off-tree ripening of two pear cultivars with different ripening patterns. Plant physiology biochemistry PPB 155, 842–850. https://doi.org/10.1016/J.PLAPHY.2020.08.018.

Lindo-García, V., Muñoz, P., Larrigaudière, C., Munné-Bosch, S., Giné-Bordonaba, J., 2020b. Interplay between hormones and assimilates during pear development and ripening and its relationship with the fruit postharvest behaviour. Plant. Sci. 291, 110339. https://doi.org/10.1016/j.plantsci.2019.110339.

Liu, M., Pirrello, J., Chervin, C., Roustan, J.-P., Bouzayen, M., 2015. Ethylene control of fruit ripening: revisiting the complex network of transcriptional regulation. Plant. Physiol. 169 23802390. https://doi.org/10.1104/pp.15.01361.

Mangaraj, S., Goswami, T.K., 2011. Modeling of respiration rate of litchi fruit under aerobic conditions. Food Bioprocess. Technol. 4, 272–281. https://doi.org/10.1007/s11947-008-0145-z.

Mditshwa, A., Fawole, O.A., Opara, U.L., 2018. Recent developments on dynamic controlled atmosphere storage of apples—a review. Food Packag. Shelf Life 16, 59–68. https://doi.org/10.1016/j.fpsl.2018.01.011.

Nguyen, T.M.V., Tran, D.T., Mata, C.I., Van de Poel, B., Nicolaï, B.M., Hertog, M.L.A.T.M., 2025. Gene expression driving ethylene biosynthesis and signaling pathways in ripening tomato fruit; a kinetic modelling approach. J. Exp. Bot. eraf055. https://doi.org/10.1093/jxb/eraf055.

Pattyn, J., Vaughan-Hirsch, J., Van de Poel, B., 2021. The regulation of ethylene biosynthesis: a complex multilevel control circuitry. New. Phytol. 229, 770–782. https://doi.org/10.1111/nph.16873.

Peppelenbos, H.W., Van'T Leven, J., 1996. Evaluation of four types of inhibition for modelling the influence of carbon dioxide on oxygen consumption of fruits and vegetables. Postharvest Biol. Technol. 7, 27–40. https://doi.org/10.1016/0925-5214(96)80995-1.

Phan, H.M., Hertog, M.L.A.T.M., Verlinden, B.E., Verboven, P., Nicolaï, B.M., 2026a. Dynamic change in respiration rate of 'Conference' pear in DCA storage: experimental evidence and modeling. Acta Hortic. 179–184. https://doi.org/10.17660/ActaHortic.2026.1456.23.

Phan, H.M., Verlinden, B.E., Hertog, M.L.A.T.M., Verboven, P., Nicolai, B.M., 2026b. Improving energy efficiency in pear storage through dynamic controlled atmosphere (DCA). Int. J. Refrig. 182, 447–455. https://doi.org/10.1016/j.ijrefrig.2025.12.015.

Prange, R.K., 2018. Dynamic controlled atmosphere (DCA) storage of fruits and vegetables. Ref. Modul. Food Sci. https://doi.org/10.1016/b978-0-08-100596-5.21349-8.

Rogge, S., Defraeye, T., Herremans, E., Verboven, P., Nicolaï, B.M., 2015. A 3D contour based geometrical model generator for complex-shaped horticultural products. J. Food Eng. 157, 24–32. https://doi.org/10.1016/j.jfoodeng.2015.02.006.

Saltveit, M.E., 2003. Is it possible to find an optimal controlled atmosphere? Postharvest Biol. Technol. 27, 3–13. https://doi.org/10.1016/S0925-5214(02)00184-9.

Saquet, A.A., Almeida, D.P.F., 2017. Ripening physiology and biochemistry of 'Rocha' pear as affected by ethylene inhibition. Postharvest Biol. Technol. 125, 161–167. https://doi.org/10.1016/J.POSTHARVBIO.2016.11.008.

Saquet, A.A., Streif, J., 2017. Respiration rate and ethylene metabolism of 'jonagold' apple and 'conference' pear under regular air and controlled atmosphere. Bragantia 76, 335–344. https://doi.org/10.1590/1678-4499.189.

Sari, M., Bahceci, I., Dogrusoz, U., Sumer, S.O., Aksoy, B.A., Babur, Ö., Demir, E., 2015. SBGNViz: a tool for visualization and complexity management of SBGN process description maps. PLoS. ONE 10, e0128985. https://doi.org/10.1371/journal.pone.0128985.

Saucedo, O., Laubmeier, A., Tang, T., Levy, B., Asik, L., Pollington, T., Feldman, O.P., 2024. Comparative analysis of practical identifiability methods for an SEIR model. MATH 9, 24722–24761. https://doi.org/10.3934/math.20241204.

Schenk, A., 2024. Bewaarcondities Appel en Peer [WWW Document]. vcbt.be. URL https://vcbt.be/bewaarcondities_appel_en_peer/ (accessed 3.5.25).

Sousa, A.R., Oliveira, J.C., Sousa-Gallagher, M.J., 2017. Determination of the respiration rate parameters of cherry tomatoes and their joint confidence regions using closed systems. J. Food Eng. 206, 13–22. https://doi.org/10.1016/j.jfoodeng.2017.02.026.

Thewes, Fabio Rodrigo, Brackmann, A., Both, V., Anese, R.D.O., Schultz, E.E., Ludwig, V., Wendt, L.M., Berghetti, M.R.P., Thewes, Flavio Roberto, 2020. Dynamic controlled atmosphere based on carbon dioxide production (DCA – CD): lower oxygen limit establishment, metabolism and overall quality of apples after long-term storage. Postharvest Biol. Technol. 168, 111285. https://doi.org/10.1016/j.postharvbio.2020.111285.

Tipu, M.M.H., Sherif, S.M., 2024. Ethylene and its crosstalk with hormonal pathways in fruit ripening: mechanisms, modulation, and commercial exploitation. Front. Plant. Sci. 15. https://doi.org/10.3389/fpls.2024.1475496.

Tucker, G., Yin, X., Zhang, A., Wang, M., Zhu, Q., Liu, X., Xie, X., Chen, K., Grierson, D., 2017. Ethylene and fruit softening. Food Qual. Saf. 1, 253–267. https://doi.org/10.1093/FQSAFE/FYX024.

Van de Poel, B., Bulens, I., Hertog, M.L.A.T.M., Nicolaï, B.M., Geeraerd, A.H., 2014. A transcriptomics-based kinetic model for ethylene biosynthesis in tomato (Solanum lycopersicum) fruit: development, validation and exploration of novel regulatory mechanisms. New. Phytol. 202, 952–963. https://doi.org/10.1111/nph.12685.

Van de Poel, B., Bulens, I., Markoula, A., Hertog, M.L.A.T.M., Dreesen, R., Wirtz, M., Vandoninck, S., Oppermann, Y., Keulemans, J., Hell, R., Waelkens, E., De Proft, M.P., Sauter, M., Nicolaï, B.M., Geeraerd, A.H., 2012. Targeted systems biology profiling of tomato fruit reveals coordination of the yang cycle and a distinct regulation of ethylene biosynthesis during postclimacteric ripening. Plant. Physiol. 160, 1498–1514. https://doi.org/10.1104/pp.112.206086.

Verlinden, B.E., Bessemans, N., Verboven, P., Nicolaï, B.M., 2023. Saving energy using RQ-based dynamic controlled atmosphere storage of blueberry fruit., in: Proceedings of the 26th IIR International Congress of Refrigeration: Paris, France, August 21-25, 2023. https://doi.org/10.18462/iir.icr.2023.0954.

Verreydt, C., Verboven, P., Defraeye, T., Piovesan, A., ElGamal, R., Van De Looverbosch, T., Hertog, M., Nicolaï, B., 2022. Multiscale modeling of RQ-DCA storage of different pear cultivars using a hybrid physics-based stochastic approach. Postharvest Biol. Technol. 194. https://doi.org/10.1016/j.postharvbio.2022.112083.

Villalobos-Acuña, M., Mitcham, E.J., 2008. Ripening of European pears: the chilling dilemma. Postharvest Biol. Technol. 49, 187–200. https://doi.org/10.1016/J.POSTHARVBIO.2008.03.003.

Villalobos-Acuña, M.G., Biasi, W.V., Flores, S., Jiang, C.Z., Reid, M.S., Willits, N.H., Mitcham, E.J., 2011. Effect of maturity and cold storage on ethylene biosynthesis and ripening in 'Bartlett' pears treated after harvest with 1-MCP. Postharvest Biol. Technol. 59, 1–9. https://doi.org/10.1016/J.POSTHARVBIO.2010.08.001.

Wang, C.Y., Mellenthin, W.M., Hansen, E., 1972. Maturation of 'Anjou' pears in relation to chemical composition and reaction to ethylene. J. Am. Soc. Hortic. Sci. 97, 9–12. https://doi.org/10.21273/JASHS.97.1.9.

Wang, Z.-W., Duan, H.-W., Hu, C.-Y., 2009. Modelling the respiration rate of guava (Psidium guajava L.) fruit using enzyme kinetics, chemical kinetics and artificial neural network. Eur. Food Res. Technol. 229, 495–503. https://doi.org/10.1007/s00217-009-1079-z.

Wendt, L.M., Ludwig, V., Thewes, F.R., Soldateli, F.J., Batista, C.B., Fukui, C.M., Gonçalves Dos Santos, G., Katsurayama, J.M., Brackmann, A., Both, V., 2024. Effect of dynamic controlled atmosphere on volatile compound profile and quality of pears. Sci. Hortic. 328, 112910. https://doi.org/10.1016/j.scienta.2024.112910.

Xiao, H., Verboven, P., Tong, S., Pedersen, O., Nicolaï, B., 2024. Hypoxia in tomato (Solanum lycopersicum) fruit during ripening: biophysical elucidation by a 3D reaction–diffusion model. Plant. Physiol. 195, 1893–1905. https://doi.org/10.1093/plphys/kiae174.

Zi, Z., 2011. Sensitivity analysis approaches applied to systems biology models. IET Syst. Biol. https://doi.org/10.1049/iet-syb.2011.0015.